

Stochastic Chern number from interactions and light response

Philipp W. Klein¹, Adolfo G. Grushin², and Karyn Le Hur¹

¹CPHT, CNRS, Ecole Polytechnique, Institut Polytechnique de Paris, Route de Saclay, 91128 Palaiseau, France and

²Institut Néel, CNRS and Université Grenoble Alpes, Grenoble, France

(Dated: April 24, 2022)

We develop a stochastic description of the topology in an interacting Chern insulator. Electron-electron interactions can produce a substantial number of particle-hole pairs above the band gap, which leads us to propose a “stochastic Chern number” as an interacting measure of the topology. We confirm the Mott transition’s first-order nature in the interacting quantum anomalous Hall effect on the honeycomb geometry, from a mean-field variational approach, supported by density matrix renormalization group results and Ginzburg-Landau arguments. From the Bloch sphere, we make predictions for circular dichroism of light related to transport properties on the lattice and suggest protocols to reveal the stochastic Chern number. We also build an analogy between interaction-induced particle-hole pairs and temperature effects. Our stochastic approach is physically intuitive, computationally easy and leads the way to further studies of interaction effects in Chern insulators.

Introduction - Topological phases of matter have attracted a lot of interest in the last years, including generalizations of the quantum Hall effect [1] to the Haldane model on the honeycomb lattice [2]. This gives rise to the quantum anomalous Hall effect which has been realized in quantum materials [3], graphene [4], photonic systems [5–10] and cold atoms in optical lattices [11, 12]. The occurrence of an insulating bulk and a protected chiral edge mode can be understood through a quantized topological number, the Chern number, assuming non-interacting particles. These systems at half-filling then behave as Chern insulators (CI). While some progress has been made in the description of interacting Chern systems, in the bosonic case [13, 14], and both for spinless [13, 15–17] and spinfull [18–22] fermions, and more generally in the description of interacting topological systems [23], several central questions remain open. In this Letter, we introduce a many-body description for interacting CIs, taking into account interaction-induced particle-hole pairs and describing Mott physics at half-filling.

To describe the effect of particle-hole pairs in the Haldane model on the honeycomb lattice with a nearest-neighbor interaction, we introduce a Hubbard-Stratonovitch transformation to re-write the quartic fermionic interaction as Gaussian variables [24], referring to stochastic variables. One stochastic variable can be identified as a Semenoff mass [25], which will produce a sign flip of the mass term at one Dirac point only at the Mott transition. Within this approach, there is a direct relation between the creation of particle-hole pairs above the band gap due to interaction effects and fluctuations of this stochastic variable around its mean value. By analogy to the studies of the two-dimensional Hubbard model [26, 27], other variables dressing the kinetic term and referring to the particle-hole channel, will also play an important role. This particle-hole channel will produce a jump of the Charge Density Wave (CDW) order parameter at the Mott transition, already at a mean-field level from a variational approach, in agreement with infinite

density matrix renormalization group (iDMRG) results. We are astonished that this particle-hole channel which provides a physical insight behind the Mott transition’s first-order nature, has not been introduced before. The phase transition was previously shown to be first-order from exact diagonalization [13, 15]. We also analyse the phase transition using a Ginzburg-Landau approach [28].

Furthermore, circular dichroism of light is related to the quantized Chern number [29, 30] for the non-interacting Haldane model. Shining light induces a population of the states in the upper band, above the band gap. The associated depletion rates depend on the orientation of the circular drive. The Chern number is encoded in the difference of rates with opposite orientation. Through a mathematical formulation on the Bloch sphere, we show that the topology of the system is already described by the depletion rates that occur at the Dirac points of the Brillouin zone. We consider interaction effects that contribute to the formation of particle-hole pairs and thereby stochastically change the Chern number as defined through the circular dichroism of light. We define the stochastic Chern number through an average of the Chern number on the ensemble of stochastic variables. We study how the stochastic topological number is linked to protocols on the Bloch sphere [31] and to the finite-temperature Chern number [32].

The model - We consider the model Hamiltonian $\mathcal{H} = \mathcal{H}_0 + \mathcal{H}_V$, where \mathcal{H}_0 is the Haldane honeycomb model for spinless fermions at half-filling [2] and \mathcal{H}_V is the nearest neighbor interaction

$$\begin{aligned} \mathcal{H}_0 &= - \sum_{\langle i,j \rangle} t_1 c_i^\dagger c_j - \sum_{\langle\langle i,j \rangle\rangle} t_2 e^{\pm i\Phi} c_i^\dagger c_j \\ \mathcal{H}_V &= V \sum_{\langle i,j \rangle} (n_i - 1/2) (n_j - 1/2). \end{aligned} \quad (1)$$

Here, t_1 represents the nearest-neighbor hopping strength which we set to unity hereafter ($t_1 = 1$). Furthermore, $t_2 e^{\pm i\Phi}$ represents the next-nearest neighbor hopping term where we fix the Peierls phase to $\Phi = \pi/2$,

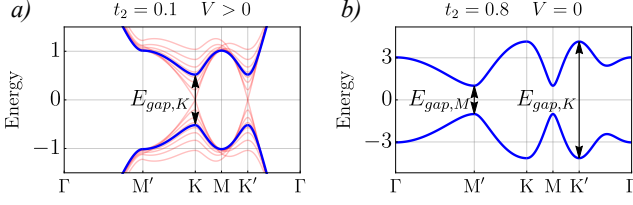


FIG. 1. (color online) (a) Band structure (blue pair of bands) for small $t_2 < 0.2$ with $t_1 = 1$. The low energy physics is centered around the Dirac points, where the stochastic approach applies. If we allow for fluctuations at $V > 0$, the sampling of ϕ^z corresponds to the creation of quasi states that change the band gap at the K and K' points. (b) Haldane band structure for large $t_2 > 0.2$ such that the low energy regime is located at the M-points.

for simplicity. Here, the positive (negative) sign refers to (counter-) clockwise hopping [33]. The energy bands in the Haldane model are represented in Fig. 1.

Previous studies [16, 17] have suggested that at a mean field level the quartic interaction term can be decoupled into a CDW order parameter which then acts as a staggered potential in sublattice space on \mathcal{H}_0 . A straightforward approach, proposed in Ref. [16], would be to rewrite \mathcal{H}_V exactly as $\mathcal{H}_V = \frac{V}{4} \sum_{\langle i,j \rangle} (n_i - n_j)^2$ in order to find a simple mean-field theory for the CDW order. Crucially however, this ansatz does not take into account the fact that the correlator $\langle c_i^\dagger c_j \rangle$, referring to the particle-hole channel [26, 27], is finite in two-dimensional Hubbard models and therefore contributes to the interaction energy $\langle c_i^\dagger c_i c_j^\dagger c_j \rangle$. When particle-hole channels are not included, one finds the Mott phase transition to be second-order [16, 17], which is not in agreement with exact diagonalization results (at finite t_2) [13].

A mean-field ansatz can be derived by rewriting the quartic term exactly as $c_i^\dagger c_i c_j^\dagger c_j = \sum_r \eta_r (c_i^\dagger \sigma_{ij}^r c_j)^2$ where σ^r are the Pauli matrices acting on sublattice space, and r represents $(0, x, y, z)$. The coefficients η_r need to be chosen such that they fulfill the three conditions $\eta_0 = -\eta_z$, and $\eta_x = \eta_y$, as well as $1/4 = \eta_0 - \eta_x$. In general, the right choice of the η_r can only be systematically computed within a variational mean-field theory. Such an ansatz aims to minimize the energy of the full, original Hamiltonian $\langle \mathcal{H} \rangle$ with respect to the ground state of some trial Hamiltonian [33]. We find that the choice $\eta_0 = -\eta_{x,y,z} = \frac{1}{8}$ minimizes the energy.

We can then write down the partition function and action for the Hamiltonian \mathcal{H} and decouple the quartic interaction by performing a Hubbard-Stratonovich transformation [24, 34] for each r , so e.g. for $r \in (x, y, z)$ as $e^{\frac{V}{8} \sum_{i,p} (c_i^\dagger \sigma_{i,p}^r c_{i+p})^2} = \int D\phi^r e^{-\sum_{i,p} 2V(\phi_{i+p/2}^r)^2 + V\phi_{i+p/2}^r (c_i^\dagger \sigma_{i,p}^r c_{i+p})}$ where i denotes a unit cell, $p \in (x, y, z)$, and we introduced an auxiliary field $\phi_{i+p/2}^r$ on each link between lattice sites i (sublattice A) and $i+p$ (sublattice B). The auxiliary-field variables are time-independent. Although we choose

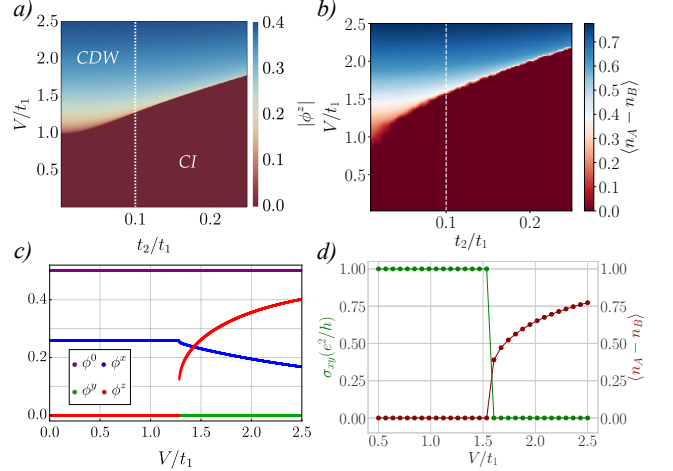


FIG. 2. (color online) (a) $V - t_2$ mean field phase diagram from the method. The transition marks the condensation of the CDW order parameter ϕ^z . (b) Same phase diagram obtained with iDMRG. (c) Absolute value of the self-consistent ϕ^r variable as a function of V for $t_2 = 0.1$. (d) Hall conductivity and $\langle n_A - n_B \rangle$ from iDMRG.

a decoupling ansatz similar to that of a quantum Monte Carlo approach [35], we do not experience the sign problem present in the interacting Haldane model since we do not sample the auxiliary fields in imaginary time. Through the Parseval-Plancherel theorem, our approach is equivalent to set the frequency to zero (see [33]), which is justified related to ground-state properties.

After switching to Fourier space, we aim to build an effective model at the Dirac points. We keep the leading scattering contribution around each Dirac point. Finally, we derive the effective mean-field Hamiltonian $\mathcal{H}_{\text{mf}} = \sum_{\mathbf{k}} \Psi_{\mathbf{k}}^\dagger \mathcal{H}_{\text{mf}}^{\mathbf{k}} \Psi_{\mathbf{k}}$, where $\Psi_{\mathbf{k}}^\dagger = (c_{\mathbf{k}A}^\dagger, c_{\mathbf{k}B}^\dagger)$ is the spinor basis acting on sublattice A and sublattice B of the honeycomb lattice respectively (see [33]), for each wavevector \mathbf{k} and

$$\mathcal{H}_{\text{mf}}^{\mathbf{k}} = \begin{pmatrix} \gamma(\mathbf{k}) - 3V(\phi^0 + \frac{1}{2}) & -g(\mathbf{k}) \\ -g^*(\mathbf{k}) & -\gamma(\mathbf{k}) - 3V(\phi^0 + \frac{1}{2}) \end{pmatrix} \quad (2)$$

is the Hamiltonian density. We have introduced the functions $\gamma(\mathbf{k}) = 3V\phi^z - 2t_2 \sum_p \sin(\mathbf{k} \cdot \mathbf{b}_p)$, and $g(\mathbf{k}) = [t_1 - V(\phi^x + i\phi^y)] \sum_p (\cos(\mathbf{k} \cdot \mathbf{a}_p) - i \sin(\mathbf{k} \cdot \mathbf{a}_p))$. The vectors \mathbf{a}_p and \mathbf{b}_p are the nearest and next-nearest neighbor displacements, respectively [33]. The field ϕ^0 can be absorbed in the chemical potential and will be fixed to $\phi^0 = -1/2$ at half-filling. The field ϕ^z changes sign in sublattice space and therefore plays the role of a staggered chemical potential. On the one hand, it measures the particle density difference between sublattices A and B, and captures CDW order. Furthermore, it acts as a Semenoff mass term [25] on the Haldane model and therefore controls the Chern number of the system [2]. The variables ϕ^x and ϕ^y dress the nearest-neighbor hopping term and assuming t_1 is real then this favors $\phi^y = 0$ while

$\phi^x \neq 0$. The ϕ^z variable is also real in the definition of the Hubbard-Stratonovitch transformation.

In Fig. 2a), we present the two-dimensional $t_2 - V$ phase diagram obtained with a variational approach on the mean-field theory and additional information on the method can be found in the Supplementary Material [33]. We confirm the presence of two phases [13, 14], a CI phase with a perfectly quantized Chern number and a Mott or CDW phase. The CDW phase is characterized by a non-zero value of $\langle n_A - n_B \rangle$ or ϕ^z ; as long as $\langle n_A - n_B \rangle$ is not equal to unity, then ϕ^x can remain finite above the transition as a result of quantum fluctuations. Fig. 2c) shows the numerical solution of the mean field equations for $t_2 = 0.1$. The jump in the CDW order parameter ϕ^z indicates the first-order phase transition. In the Supplemental Material [33], we also show the evolution of the CDW jump as a function of t_2 , and we develop a Ginzburg-Landau analysis which supports the first-order nature of the transition.

iDMRG results - We have compared our mean field calculations with simulations using the infinite density matrix renormalization group (iDMRG) by means of the python package TENPY [36], written in the language of matrix product states. This numerical method calculates the ground-state of the model (1) in the infinite cylinder geometry, as well as the expectation of the CDW order parameter, $\langle n_A - n_B \rangle$, the Hall conductivity σ_{xy} , the correlation length ξ and the entanglement entropy S . The bond dimension χ is a measure of the maximum number of states kept by the algorithm, and sets the accuracy of the calculation. We have performed calculations up to $\chi = 1200$ for cylinder circumferences of $L_y = 6, 12$ sites and our results show good convergence for bond dimensions as low as $\chi \gtrsim 200$, consistent with previous iDMRG calculations [37] (see [33]).

The phase diagram for $\chi = 200$ and $L_y = 6$ is shown in Fig. 2b). In Fig. 2d) we show the CDW order parameter and the Hall conductivity along a cut at $t_2/t_1 = 0.1$, which show a discontinuity along the transition for all χ s. These discontinuities are typical of a first-order phase transition, further supported by the saturation of the entanglement entropy at the transition as a function of correlation length (see [33]). Comparing iDMRG results with the mean-field variational approach, our findings agree as long as the smallest band gap (relevant energy scale for CDW order) is located at the K-points (relevant for topology), which is the case for $t_2 \leq 0.2$ [33]. Therefore, we focus on this parameter regime.

Circular dichroism of light - Now, we address the light responses of the CI to circularly polarized light with different polarizations [29]. First, resorting to a Bloch sphere argument where the light-matter coupling is defined through the introduction of a time-dependent vector potential in Eq. (2) above [33], we show that topology can be described from the light-matter coupling at the K and K' points only and we build a link with the

transport properties on the lattice. The depletion rates $\Gamma_{l \rightarrow u}^{\pm}(\mathbf{k} = \mathbf{K}, \mathbf{K}')$ encode the mass term $|m| = 6\sqrt{3}t_2$ which determines the size of the band gap at the K-points. The next-nearest neighbor hopping term $t_2 e^{i\Phi}$ breaks time-reversal symmetry, and leads to different signs of m at the K and K' points, and therefore, to non-trivial topology [2]. We also show the relation between the Bloch sphere arguments and with the depletion rates as derived in Ref. [29] from Fermi's golden rule:

$$\Gamma_{l \rightarrow u}^{\pm}(\omega_{\mathbf{k}}, \mathbf{k}) = \frac{2\pi}{\hbar} \left(\frac{E}{\hbar\omega} \right)^2 |\mathcal{A}_{l \rightarrow u}^{\pm}|^2 \delta(\epsilon_u^{\mathbf{k}} - \epsilon_l^{\mathbf{k}} - \hbar\omega) \quad (3)$$

and $\Gamma_{l \rightarrow u}^{\pm}(\omega_{\mathbf{k}}) = \sum_{\mathbf{k} \in \text{BZ}} \Gamma_{l \rightarrow u}^{\pm}(\omega_{\mathbf{k}}, \mathbf{k})$. Here, the transition amplitude is given by $\mathcal{A}_{l \rightarrow u}^{\pm} = \langle u_{\mathbf{k}} | \frac{1}{i} \frac{\partial \mathcal{H}_0}{\partial k_x} \mp \frac{\partial \mathcal{H}_0}{\partial k_y} | l_{\mathbf{k}} \rangle$, E is the strength of the drive or the electric field in the original basis, $|u_{\mathbf{k}}\rangle$ and $|l_{\mathbf{k}}\rangle$ are the eigenstates corresponding to the lower and upper bands, $\epsilon_{l,u}^{\mathbf{k}}$ their eigenenergies, and the \pm selects the polarization orientation. Within the Fermi golden rule, it's equivalent to sum on all the momenta \mathbf{k} in the entire Brillouin zone as in Ref. [29], or just consider the Dirac points only (see [33]). We check numerically that we can evaluate the Chern number in the non-interacting Haldane model with the formula at the Dirac points only, and find for the frequency-integrated rates

$$\frac{1}{2} \int_0^{\infty} d\omega \sum_{\mathbf{k} = \mathbf{K}, \mathbf{K}'} \Gamma_{l \rightarrow u}^{+}(\omega_{\mathbf{k}}, \mathbf{k}) - \Gamma_{l \rightarrow u}^{-}(\omega_{\mathbf{k}}, \mathbf{k}) = \rho C \quad (4)$$

with the constant $\rho = 16\pi^3 E^2 \sqrt{3} |t_1|^2 m^{-2}$. In the non-interacting case, C is one in the topological non-trivial phase of the Haldane model and exactly zero otherwise, and is thus the (ground state) Chern number. The prefactor $1/m^2$ comes from Eq. (3) written in terms of E .

Eq. (3) is also applicable in the presence of interactions within the mean-field variational approach and through this formula we show that the light responses can probe the jump in the Chern number at the Mott transition for the ground state (see [33]). Computing the circular dichroism of light for the entire Brillouin zone gives the numerical result of Figs. 3a)-3d). Although both Figs. 3a) and 3b) show the same ground state Chern number, the difference between the two reveals the effect of the particle-hole channel ϕ^x . Increasing V renormalizes t_1 . Considering Fig. 3c), the sign flip of the mass term at one K-point at the CDW transition is reflected by regions of blue curve (Γ^+) turning light red (Γ^-).

Stochastic Chern number and Measures - When V approaches the size of the smallest band gap around the K-points in Fig. 1a), particle-hole pair excitations will start to form. This leads to the formation of a mixed state which is described below through fluctuations of the stochastic variables around their mean values. We consider Eq. (4) and substitute $\mathcal{H}_0 \rightarrow \mathcal{H}^{\text{mf}}$. The auxiliary fields ϕ^r are mathematically Gaussian random variables $P(\phi^r) = (1/\sqrt{2\pi\xi(V)}) \exp(-\frac{1}{2}(\phi^r - \phi_{\text{mf}}^r)^2 \xi^{-1}(V))$

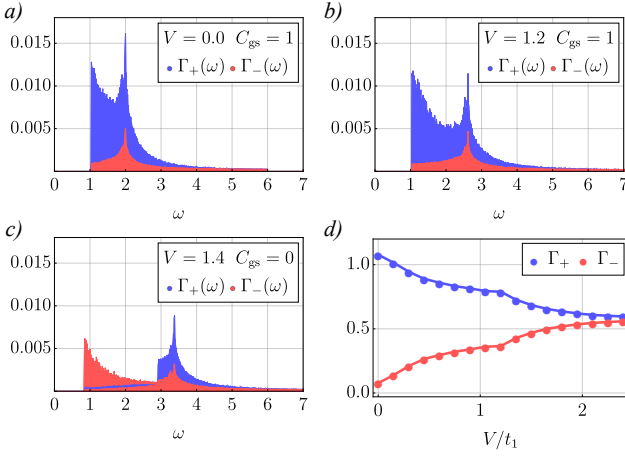


FIG. 3. (color online) (a-c) Ground state depletion rate $\Gamma_{\pm} \equiv \sum_{\mathbf{k} \in \text{BZ}} \Gamma_{l \rightarrow u}^{\pm}(\omega_{\mathbf{k}}, \mathbf{k})$ as a function of frequency for $t_2 = 0.1$ and different fixed values of the interaction strength V . (d) Stochastic frequency-integrated depletion rate $\Gamma_{\pm} \equiv \frac{1}{2} \rho^{-1} \int d\omega \sum_{\mathbf{k} \in \mathbf{K}, \mathbf{k}'} \Gamma_{l \rightarrow u}^{\pm}(\omega_{\mathbf{k}}, \mathbf{k})$ as a function of V .

where $\xi(V) = (1/12V)$, and the mean of the Gaussian distribution is given by the mean-field solution ϕ_{mf}^r . Importantly, ϕ^z acts as Semenoff mass term on the Haldane model modifying the band gap at the Dirac points. More precisely, sampling ϕ^z around the saddle point solution generates excited states with smaller energy band gaps, see the light red bands in Fig. 1a). We sample the fields $(\phi^x, \phi^y, \phi^z) = \phi$ according to $P(\phi^r)$ while keeping the chemical potential ϕ^0 constant at half-filling. In Fig. 3d), we show the evolution of the ensemble-averaged rates Γ_+ and Γ_- as a function of V , when sampling on the stochastic variables ϕ . These variables are now hidden in the eigenenergies in Eq. (3).

For each configuration we can also compute a ϕ -dependent Chern number $C(\phi)$ via Eq. (4) that will be either one or zero. As the term $3V\phi^z$ plays the role of a Semenoff mass term acting on the Haldane model, we can define - for a given $V - \phi_c^z$ such that $3V|\phi_c^z| = 3\sqrt{3}t_2$. Then, all states with $|\phi^z| < |\phi_c^z|$ produce a Chern number $C(\phi) = 1$ to C_{st} while all other $|\phi^z|$ contribute zero. Then, we propose to define the *stochastic Chern number*

$$C_{\text{st}} \equiv \int_{-\infty}^{+\infty} d\phi P(\phi) C(\phi), \quad (5)$$

which can take non-integer values when it refers to a mixed state. In the limit where $V \rightarrow 0^+$, C_{st} agrees with the definition of the non-interacting topological invariant C . Furthermore, the stochastic variables remain pinned to their ground state values when $V \rightarrow 0^+$, in accordance with $\phi_c^z \rightarrow +\infty$. Computing C_{st} for 10^5 random configurations, as a function of V , then we obtain the result in red in Fig. 4a), which can be compared to the ground state Chern number C_{gs} in blue obtained when $\phi^z = \phi_{\text{mf}}^z$. The quantity C_{gs} determines the quantum Hall conductivity, in agreement with iDMRG (see Fig. 2d) and with

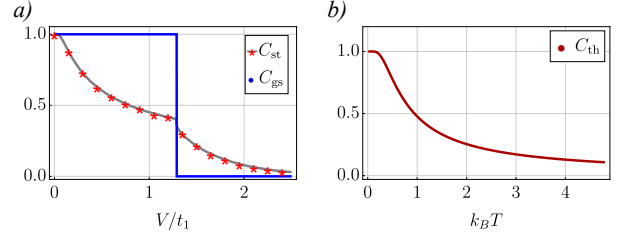


FIG. 4. (color online) (a) Evaluation of the ground state Chern number C_{gs} and stochastic Chern number C_{st} as a function of V . The grey curve comes from an analytical formula. (b) C_{th} from Eq. (6) at $V = 0$ as a function of $k_B T$.

the Bloch sphere arguments ([33]). Hence, we can derive C_{st} also via $C_{\text{st}} = \int_{-|\phi_c^z|}^{+|\phi_c^z|} d\phi^z P(\phi^z) \approx 1 - 2P(|\phi^z| \sim |\phi_c^z|)$ which results in the grey curve in Fig. 4a). This relation then ensures the correspondence between the ensemble-averaged values of $\Gamma_+ - \Gamma_-$ in Fig. 3d), and C_{st} as a function of V . We note that C_{st} still reveals the first-order Mott transition through a small jump in Fig. 4a).

We can now formulate an analogy with the finite-temperature version of the Hall conductivity [32] and introduce a finite-temperature version of Eq. (4)

$$\frac{1}{2} \int_0^{\infty} d\omega \sum_{\alpha, \mathbf{k}} p^{\mathbf{k}} \Gamma_{\alpha}^+ (\omega_{\mathbf{k}}, \mathbf{k}) - p^{\mathbf{k}} \Gamma_{\alpha}^- (\omega_{\mathbf{k}}, \mathbf{k}) = \rho C_{\text{th}} \quad (6)$$

where $p^{\mathbf{k}} = (1 + \exp(\epsilon_{u,l}^{\mathbf{k}}/k_B T))^{-1}$ is the Fermi distribution, k_B is the Boltzmann constant, and the variable α here refers to $\{l \rightarrow u, u \rightarrow l\}$ such that $p^{\mathbf{k}}$ effectively mixes the states of the lower and upper band. In the description of Eq. (3), we take the Fermi occupancies into account through the replacement $E^2 \rightarrow E^2 p^{\mathbf{k}}$, implying that if a state is unoccupied then this state cannot couple to light. We then allow in Eq. (6) for heating of the bulk to contribute to C_{th} [32]. From Eq. (6), we find that at low temperatures ($k_B T \ll m$), the finite-temperature Chern number C_{th} decreases smoothly as $1 - e^{-m/k_B T}$ in Fig. 4 [33]. In the presence of interactions, we observe that the probability to create a particle-hole pair in the topological phase will be dominated by values of $|\phi^z| \sim |\phi_c^z|$, producing a reduction of C_{st} evolving as $P(|\phi^z| \sim |\phi_c^z|) \propto e^{-m^2/(k_B T_{\text{eff}})^2}$ with an effective temperature such that $k_B T_{\text{eff}} \propto \sqrt{V}$ in Fig. 4. We propose two protocols from the Bloch sphere, one related to circular dichroism of light and one from a path linking the north and south poles, to measure T_{eff} [33]. Very recently, it was also suggested to probe similar effects through a non-adiabatic quantum Hall response [38].

Conclusion - We have introduced a variational topological mean-field theory to describe interaction effects in the fermionic Haldane model with nearest-neighbor interactions. We have then shown how interaction-induced particle-hole pairs can be described through stochastic variables encoding fluctuations around the mean-field theory. The method could be generalized in various direc-

tions, such as bilayer systems [39] and the Kane-Mele [40–42] model and lead to further insight on probing particle-hole pairs’ responses in interacting topological systems.

Acknowledgements - We acknowledge discussions with N. Regnault, S. Biermann, M. O. Goerbig, G. Uhrig, C. Weitenberg, N. Goldman, W. Wu, A. Rosch, J. Hutchinson, C. Repellin, L. Herviou and H.-Y. Sit. This research was funded by the Deutsche Forschungsgemeinschaft (DFG, German Research Foundation) via Research Unit FOR 2414 under project number 277974659 (PWK and KLH). Furthermore, KLH acknowledges funding from the French ANR BOCA and from CIFAR in Canada. AGG is supported by the ANR JCJC ANR-18-CE30-0001-01.

[1] K. v. Klitzing, G. Dorda, and M. Pepper, *Phys. Rev. Lett.* **45**, 494 (1980).

[2] F. D. M. Haldane, *Phys. Rev. Lett.* **61**, 2015 (1988).

[3] C.-X. Liu, S.-C. Zhang, and X.-L. Qi, *Annual Review of Condensed Matter Physics* **7**, 301 (2016).

[4] J. W. McIver, B. Schulte, F.-U. Stein, T. Matsuyama, G. Jotzu, G. Meier, and A. Cavalleri, *Nature Physics* (2019), 10.1038/s41567-019-0698-y.

[5] F. D. M. Haldane and S. Raghu, *Phys. Rev. Lett.* **100**, 013904 (2008).

[6] L. Lu, J. D. Joannopoulos, and M. Soljacic, *Nature Photonics* **8**, 821 (2014).

[7] M. C. Rechtsman, J. M. Zeuner, Y. Plotnik, Y. Lumer, D. Podolsky, F. Dreisow, S. Nolte, M. Segev, and A. Szameit, *Nature* **496**, 196 (2013).

[8] J. Koch, A. A. Houck, K. Le Hur, and S. M. Girvin, *Phys. Rev. A* **82**, 043811 (2010).

[9] K. Le Hur, L. Henriet, A. Petrescu, K. Plekhanov, G. Roux, and M. Schiro, *Comptes Rendus Physique* **17**, 808 (2016).

[10] T. Ozawa, H. M. Price, A. Amo, N. Goldman, M. Hafezi, L. Lu, M. C. Rechtsman, D. Schuster, J. Simon, O. Zilberman, and I. Carusotto, *Rev. Mod. Phys.* **91**, 015006 (2019).

[11] G. Jotzu, M. Messer, R. Desbuquois, M. Lebrat, T. Uehlinger, D. Greif, and T. Esslinger, *Nature* **515**, 237 (2014).

[12] N. Flaschner, B. S. Rem, M. Tarnowski, D. Vogel, D.-S. Luhmann, K. Sengstock, and C. Weitenberg, *Science* **352**, 1091 (2016).

[13] C. N. Varney, K. Sun, M. Rigol, and V. Galitski, *Phys. Rev. B* **82**, 115125 (2010).

[14] I. Vasić, A. Petrescu, K. Le Hur, and W. Hofstetter, *Phys. Rev. B* **91**, 094502 (2015).

[15] C. N. Varney, K. Sun, M. Rigol, and V. Galitski, *Phys. Rev. B* **84**, 241105 (2011).

[16] L. Wang, H. Shi, S. Zhang, X. Wang, X. Dai, and X. C. Xie, “Charge-density-wave and topological transitions in interacting haldane model,” (2010), arXiv:1012.5163 [cond-mat.str-el].

[17] E. Alba, J. K. Pachos, and J. J. García-Ripoll, *New Journal of Physics* **18**, 033022 (2016).

[18] C. Hickey, P. Rath, and A. Paramekanti, *Phys. Rev. B* **91**, 134414 (2015).

[19] J. Maciejko and A. Rüegg, *Phys. Rev. B* **88**, 241101 (2013).

[20] D. Prychynenko and S. D. Huber, *Physica B: Condensed Matter* **481**, 53 (2016).

[21] J. Imriška, L. Wang, and M. Troyer, *Phys. Rev. B* **94**, 035109 (2016).

[22] T. I. Vanhala, T. Siro, L. Liang, M. Troyer, A. Harju, and P. Törmä, *Phys. Rev. Lett.* **116**, 225305 (2016).

[23] S. Rachel, *Reports on Progress in Physics* **81**, 116501 (2018).

[24] H. J. Schulz, “Functional integrals for correlated electrons,” (1994), arXiv:cond-mat/9402103 [cond-mat].

[25] G. W. Semenoff, *Phys. Rev. Lett.* **53**, 2449 (1984).

[26] P. W. Anderson, P. A. Lee, M. Randeria, T. M. Rice, N. Trivedi, and F. C. Zhang, *J Phys. Condens. Matter* **16**, R755 (2004).

[27] K. Le Hur and T. M. Rice, *Annals of Physics* **324**, 1452 (2009).

[28] V. L. Ginzburg and L. D. Landau, *Zh. Eksp. Teor. Fiz.* **20**, 1064 (1950).

[29] D. T. Tran, A. Dauphin, A. G. Grushin, P. Zoller, and N. Goldman, *Science Advances* **3**, e1701207 (2017).

[30] L. Asteria, D. T. Tran, T. Ozawa, M. Tarnowski, B. S. Rem, N. Flaschner, K. Sengstock, N. Goldman, and C. Weitenberg, *Nature Physics* **15**, 449 (2019).

[31] J. Hutchinson and K. Le Hur, arXiv:2002.11823 (2020).

[32] A. Rivas, O. Viyuela, and M. A. Martin-Delgado, *Phys. Rev. B* **88**, 155141 (2013).

[33] In the supplemental material, we provide further information on the lattice structure, the path integral calculation, variational mean-field theory, the energetic and Ginzburg-Landau analysis, the circular dichroism of light at the Dirac points and relation with transport properties on the lattice, protocols to measure the stochastic Chern number and further details on the iDMRG computation.

[34] A. Altland and B. D. Simons, *Condensed Matter Field Theory*, 2nd ed. (Cambridge University Press, 2010).

[35] D. Zheng, G.-M. Zhang, and C. Wu, *Phys. Rev. B* **84**, 205121 (2011).

[36] J. Hauschild and F. Pollmann, *SciPost Phys. Lect. Notes* **5** (2018).

[37] A. G. Grushin, J. Motruk, M. P. Zaletel, and F. Pollmann, *Phys. Rev. B* **91**, 035136 (2015).

[38] M. Wei-Yuan Tu, C. Li, H. Yu, and W. Yao, *2D Materials* **7** (2020).

[39] P. Cheng, P. W. Klein, K. Plekhanov, K. Sengstock, M. Aidelsburger, C. Weitenberg, and K. Le Hur, *Phys. Rev. B* **100**, 081107 (2019).

[40] C. L. Kane and E. Mele, *Phys. Rev. Lett.* **95**, 226801 (2005).

[41] S. Rachel and K. Le Hur, *Phys. Rev. B* **82**, 075106 (2010).

[42] W. Wu, S. Rachel, W.-M. Liu, and K. Le Hur, *Phys. Rev. B* **85**, 205102 (2010).

[43] P. Coleman, *Introduction to Many-Body Physics* (Cambridge University Press, 2015).

[44] R. Agra, F. v. Wijland, and E. Trizac, *European Journal of Physics* **27**, 407?412 (2006).

[45] J. J. Binney, N. J. Dowrick, A. J. Fisher, and M. Newman, *The Theory of Critical Phenomena: An Introduction to the Renormalization Group* (Oxford University Press, Inc., New York, NY, USA, 1992).

[46] S. Capponi, *Journal of Physics: Condensed Matter* **29**, 043002 (2016).

[47] P. Hohenberg and A. Krekhov, *Physics Reports* **572**, 1 (2015).

[48] S. R. White, *Phys. Rev. B* **48**, 10345 (1993).

[49] M. P. Zaletel, R. S. K. Mong, and F. Pollmann, *Journal of Statistical Mechanics: Theory and Experiment* **2014**, P10007 (2014).

[50] J. A. Kjäll, M. P. Zaletel, R. S. K. Mong, J. H. Bardarson, and F. Pollmann, *Phys. Rev. B* **87**, 235106 (2013).

[51] J. Motruk, A. G. Grushin, F. de Juan, and F. Pollmann, *Phys. Rev. B* **92**, 085147 (2015).

[52] C. Repellin, Y.-C. He, and F. Pollmann, *Phys. Rev. B* **96**, 205124 (2017).

HONEYCOMB LATTICE STRUCTURE AND NOTATION

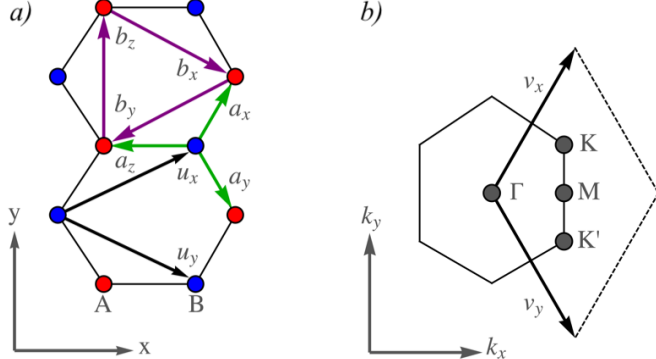


FIG. 5. (color online) (a) Honeycomb lattice in real space with sublattices A and B, lattice vectors, and (next-) nearest neighbor displacements. (b) Honeycomb lattice in momentum space, marking the Brillouin zone, reciprocal lattice vectors and high symmetry points.

First of all, we specify our conventions for the honeycomb lattice and our notation used in the main text, see Fig. 5. The set of lattice vectors is given by

$$\mathbf{u}_x = \frac{1}{2} (3, \sqrt{3}), \quad \mathbf{u}_y = \frac{1}{2} (3, -\sqrt{3}), \quad \mathbf{u}_z = (0, 0). \quad (7)$$

Here, the bond length has been set to unity in order to simplify the notation. Moreover, the nearest neighbor displacements on the honeycomb lattice are given by the set of vectors

$$\mathbf{a}_x = \frac{1}{2} (1, \sqrt{3}), \quad \mathbf{a}_y = \frac{1}{2} (1, -\sqrt{3}), \quad \mathbf{a}_z = \frac{1}{2} (-1, 0). \quad (8)$$

We can then express the next-nearest neighbor displacements on the honeycomb lattice in terms of the \mathbf{a}_p as $\mathbf{b}_i = \mathbf{a}_j - \mathbf{a}_k$ where the tuple (i, j, k) is a permutation of the bond-tuple (x, y, z) . As pointed out in previous works [39], the \mathbf{a}_p basis does not yield a Hamiltonian in Bloch form. Rather, we perform a gauge transform the Hamiltonian to a new basis, given by the lattice vectors \mathbf{u}_i , see Fig. 5.

The Brillouin zone of momentum space is visualized in Fig. 5b) and shows the high symmetry M- and K-points of the Brillouin zone. Specifically, the high symmetry Dirac-points are located at

$$\mathbf{K} = \frac{2\pi}{3} \left(1, \frac{1}{\sqrt{3}} \right), \quad \mathbf{K}' = \frac{2\pi}{3} \left(1, -\frac{1}{\sqrt{3}} \right). \quad (9)$$

HUBBARD-STRATONOVICH DECOUPLING OF THE NEAREST NEIGHBOR INTERACTION

In this work, we consider the spinless Haldane honeycomb model at half filling with nearest neighbor interactions. The model Hamiltonian is composed of two parts $\mathcal{H} = \mathcal{H}_0 + \mathcal{H}_V$ which read explicitly

$$\mathcal{H}_0 = - \sum_{\langle i,j \rangle} t_1 c_i^\dagger c_j - \sum_{\langle\langle i,j \rangle\rangle} t_2 e^{\pm i\Phi} c_i^\dagger c_j, \quad \mathcal{H}_V = V \sum_{\langle i,j \rangle} \left(n_i - \frac{1}{2} \right) \left(n_j - \frac{1}{2} \right), \quad (10)$$

where \mathcal{H}_0 is the Haldane honeycomb model in real space with nearest neighbor hopping amplitude t_1 , complex next-nearest neighbor hopping amplitude $t_2 e^{\pm i\Phi}$, and fixed Peierls phase $\Phi = \frac{\pi}{2}$. Furthermore, \mathcal{H}_V denotes the nearest neighbor interaction with interaction strength V .

In order to prepare the decoupling of the quartic interaction term, we can write \mathcal{H}_V exactly as

$$\mathcal{H}_V = V \sum_{i,p} \left(n_i - \frac{1}{2} \right) \left(n_{i+p} - \frac{1}{2} \right) = V \sum_{i,p,r} \eta_r \left(c_i^\dagger \sigma_{i,i+p}^r c_{i+p} \right)^2 - \frac{V}{2} \sum_{i,p} \left(c_i^\dagger c_i + c_{i+p}^\dagger c_{i+p} - \frac{1}{2} \right), \quad (11)$$

where i denotes a unit cell, p runs over the links (x, y, z) , r runs over $(0, x, y, z)$ and σ^r denotes the Pauli matrices acting on sublattice space with basis $(i(A), i+p(B))$. The coefficients η_r need to fulfill the relations

$$\eta_0 = -\eta_z, \quad \eta_x = \eta_y, \quad \frac{1}{4} = \eta_0 - \eta_x. \quad (12)$$

As pointed out in the main text, we need in principle to choose the η_r such that the decoupling scheme incorporates particle-hole channels (i.e. $\eta_{x,y} \neq 0$) that contribute to the total energy. A priori, a generic choice of the η_r that will ultimately minimize the total energy of the effective Hamiltonian correctly, is not obvious. Rather, a choice of coefficients η_r needs to be justified. We can set our definitions such that $\eta^z = \eta^x$, in agreement with the variational approach presented below (The self-consistent equations (32) and (34) will show the same normalization prefactors on the right-hand side of the equal sign). This approach yields the following choice of the η_r

$$-\eta_0 = \eta_x = \eta_y = \eta_z = -\frac{1}{8}. \quad (13)$$

Let us now write down the partition function and action

$$\mathcal{Z} = \int D(\Psi, \Psi^\dagger) e^{-\mathcal{S}}, \quad \mathcal{S} = \int_0^\beta d\tau \sum_{\mathbf{k}} \Psi_{\mathbf{k}}^\dagger (\partial_\tau + \mathbf{h}_0(\mathbf{k}) \cdot \boldsymbol{\sigma}) \Psi_{\mathbf{k}} + \mathcal{H}_V \quad (14)$$

where we used the spinor basis $\Psi_{\mathbf{k}}^\dagger = (c_{\mathbf{k}A}^\dagger, c_{\mathbf{k}B}^\dagger)$ to write the Haldane model in momentum space with

$$h_0^x(\mathbf{k}) = -t_1 \sum_p \cos(\mathbf{k} \cdot \mathbf{a}_p), \quad h_0^y(\mathbf{k}) = -t_1 \sum_p \sin(\mathbf{k} \cdot \mathbf{a}_p), \quad h_0^z(\mathbf{k}) = -2t_2 \sum_p \sin(\mathbf{k} \cdot \mathbf{b}_p). \quad (15)$$

Decoupling the quartic interaction term \mathcal{H}_V via a Hubbard-Stratonovich transformation for each $r \in \{x, y, z\}$ yields

$$\exp \left(\frac{V}{8} \sum_{i,p} \left(c_i^\dagger \sigma_{i,i+p}^r c_{i+p} \right)^2 \right) = \int D\phi^r \exp \left(- \sum_{i,p} 2V(\phi_{i+p/2}^r)^2 + V\phi_{i+p/2}^r \left(c_i^\dagger \sigma_{i,i+p}^r c_{i+p} \right) \right), \quad (16)$$

and for $r = 0$

$$\exp \left(-\frac{V}{8} \sum_{i,p} \left(c_i^\dagger \sigma_{i,i+p}^0 c_{i+p} \right)^2 \right) = \int D\phi^0 \exp \left(- \sum_{i,p} 2V(\phi_{i+p/2}^0)^2 + iV\phi_{i+p/2}^0 \left(c_i^\dagger \sigma_{i,i+p}^0 c_{i+p} \right) \right). \quad (17)$$

Here we introduced for each r an auxiliary field $\phi_{i+p/2}^r$ on each link between lattice sites i (on sublattice A) and $i+p$ (on sublattice B). The fields ϕ^x and ϕ^y are particle-hole channels, ϕ^0 corresponds to a chemical potential and ϕ^z to a staggered chemical potential in sublattice space that captures CDW order, but at the same time acts as a Semenoff mass term on the Haldane model and therefore controls the topological Chern number.

EFFECTIVE HAMILTONIAN

We rewrite the decoupled interaction part in Fourier space and obtain the partition function and action

$$\mathcal{Z} = \int D(\Psi, \Psi^\dagger, \phi^0, \phi^x, \phi^y, \phi^z) e^{-\mathcal{S}}, \quad (18)$$

$$\mathcal{S} = \int_0^\beta d\tau \sum_{\mathbf{k}} \Psi_{\mathbf{k}}^\dagger (\partial_\tau + \mathbf{h}_0(\mathbf{k}) \cdot \boldsymbol{\sigma}) \Psi_{\mathbf{k}} + \sum_{\mathbf{k}, \mathbf{q}, p} \Psi_{\mathbf{k}}^\dagger h_V(\mathbf{k}, \mathbf{q}, p) \Psi_{\mathbf{k}} + \sum_{\mathbf{k}, r} 6V\phi_{\mathbf{k}}^r \phi_{-\mathbf{k}}^r, \quad (19)$$

where the interaction density matrix reads

$$h_V(\mathbf{k}, \mathbf{q}, p) = V \begin{pmatrix} e^{-\frac{i}{2}(\mathbf{k}-\mathbf{q}) \cdot \mathbf{a}_p} (i\phi_{\mathbf{k}-\mathbf{q}}^0 + \phi_{\mathbf{k}-\mathbf{q}}^z) - \frac{1}{2} & e^{\frac{i}{2}(\mathbf{k}+\mathbf{q}) \cdot \mathbf{a}_p} (\phi_{\mathbf{k}-\mathbf{q}}^x - i\phi_{\mathbf{k}-\mathbf{q}}^y) \\ e^{-\frac{i}{2}(\mathbf{k}+\mathbf{q}) \cdot \mathbf{a}_p} (\phi_{\mathbf{k}-\mathbf{q}}^x + i\phi_{\mathbf{k}-\mathbf{q}}^y) & e^{\frac{i}{2}(\mathbf{k}-\mathbf{q}) \cdot \mathbf{a}_p} (i\phi_{\mathbf{k}-\mathbf{q}}^0 - \phi_{\mathbf{k}-\mathbf{q}}^z) - \frac{1}{2} \end{pmatrix}. \quad (20)$$

In principle, one could also assign an imaginary time variable τ to the stochastic variables. Applying the Parseval-Plancherel theorem, then this would result in a frequency dependence of the variables $\phi_{\mathbf{k}}^r$. Below, we develop a variational approach to evaluate the stochastic variables within the ground state properties through an energy-minimization protocol. Therefore, we consider below a time-independent, static model and therefore restrict the analysis to the zero frequency contribution. As shown in the Letter and below, for ground-state observables, this stochastic variational approach is in good agreement with the iDMRG approach. As we also show below, fluctuations of the stochastic variables around their value for the minimum of energy is well controlled. Furthermore, we restrict the discussion to leading contribution in \mathbf{k} -space for which scattering does not change momentum. Hence, we keep only the zero momentum contribution, i.e. $\mathbf{k} - \mathbf{q} = 0$. It's important to remind that sampling stochastic variables in time suffers from the sign problem for the fermionic Haldane model, which justifies our present approach. It should be emphasized that to reproduce ground-state properties, one cannot ignore the particle-hole channel ϕ^x .

The action \mathcal{S} now takes the form

$$\mathcal{S} = \sum_{\mathbf{k}} \Psi_{\mathbf{k}}^\dagger \left(\mathbf{h}_0(\mathbf{k}) \cdot \boldsymbol{\sigma} + \sum_p h_V(\mathbf{k}, p) \right) \Psi_{\mathbf{k}} + \sum_{\mathbf{k}, r} 6V \phi_{\mathbf{k}}^r \phi_{-\mathbf{k}}^r, \quad (21)$$

where the interaction density matrix now reads

$$h_V(\mathbf{k}, p) = V \begin{pmatrix} -(\phi^0 + \frac{1}{2}) + \phi^z & e^{i\mathbf{k} \cdot \mathbf{a}_p} (\phi^x - i\phi^y) \\ e^{-i\mathbf{k} \cdot \mathbf{a}_p} (\phi^x + i\phi^y) & -(\phi^0 + \frac{1}{2}) - \phi^z \end{pmatrix}. \quad (22)$$

Here we skipped the zero-momentum index of the fields, i.e. $\phi^r \equiv \phi_0^r$, and redefined the chemical potential $-i\phi^0 \rightarrow \phi^0$ such that ϕ^0 is now real for the matrix $h_V(\mathbf{k}, p)$ to be Hermitian (where it was imaginary before the substitution, such that $i\phi^0$ was real).

We set $\mathcal{H}_{\text{mf}}(\mathbf{k}) = \mathbf{h}_0(\mathbf{k}) \cdot \boldsymbol{\sigma} + \sum_p h_V(\mathbf{k}, p)$, and finally arrive at the effective mean field Hamiltonian $\mathcal{H}_{\text{mf}} = \sum_{\mathbf{k}} \Psi_{\mathbf{k}}^\dagger \mathcal{H}_{\text{mf}}(\mathbf{k}) \Psi_{\mathbf{k}}$ where the mean field Hamiltonian density in matrix form explicitly reads

$$\mathcal{H}_{\text{mf}}(\mathbf{k}) = \begin{pmatrix} \gamma(\mathbf{k}) - 3V(\phi^0 + \frac{1}{2}) & -g(\mathbf{k}) \\ -g^*(\mathbf{k}) & -\gamma(\mathbf{k}) - 3V(\phi^0 + \frac{1}{2}) \end{pmatrix}, \quad (23)$$

with the functions $\gamma(\mathbf{k})$ and $g(\mathbf{k})$ defined as

$$\gamma(\mathbf{k}) = 3V\phi^z - 2t_2 \sum_p \sin(\mathbf{k} \cdot \mathbf{b}_p), \quad (24)$$

$$g(\mathbf{k}) = [t_1 - V(\phi^x + i\phi^y)] \sum_p (\cos(\mathbf{k} \cdot \mathbf{a}_p) - i \sin(\mathbf{k} \cdot \mathbf{a}_p)). \quad (25)$$

The term $3V\phi^z$ assumes the role of a Semenoff mass term in the Haldane model, whereas the fields ϕ^x and ϕ^y renormalize the nearest neighbor hopping amplitude t_1 .

SELF CONSISTENT MEAN FIELD EQUATIONS FROM A VARIATIONAL APPROACH

Before deriving the self-consistent equations of the mean field Hamiltonian Eq. (23), we provide a general remark on the derivation of self-consistent mean field equations in the context of Hubbard-Stratonovich transformations.

Consider some general Hamiltonian $\mathcal{H} = \mathcal{H}_t + \mathcal{H}_{\text{Int}}$ with a quadratic, kinetic part H_t and a quartic interaction part of the form $H_{\text{Int}} = -\sum_{i,j} U_{ij} c_i^\dagger c_i c_j^\dagger c_j \equiv -\sum_{i,j} n_i U_{ij} n_j$ with interaction matrix U_{ij} . The quartic term can be decoupled by means of a Hubbard-Stratonovich transformation as [24, 34]

$$\exp(n_i U_{ij} n_j) = \int d\phi \exp(-\phi^i U_{ij} \phi^j - 2\phi^i U_{ij} n_j), \quad (26)$$

where we introduced some Gaussian auxiliary variable ϕ . From the partition function and action

$$\mathcal{Z} = \int D(c, c^\dagger, \phi) \exp(-\mathcal{S}), \quad \mathcal{S} = \int_0^\beta d\tau \sum_{i,j} c_i^\dagger (\partial_\tau + h_t) c_j + \phi^i U_{ij} \phi^j + 2\phi^i U_{ij} n_j, \quad (27)$$

one then usually [34, 43] computes the self consistent mean field equations via

$$\left\langle \frac{\delta \mathcal{S}}{\delta \phi^i} \right\rangle \stackrel{!}{=} 0, \quad (28)$$

which would yield in the above example

$$0 = \langle U_{ij} \phi^j + 2U_{ij} n_j \rangle, \quad \Rightarrow \quad \phi^j = -2 \langle n_j \rangle. \quad (29)$$

Now, the problem is that this result is not unique. The auxiliary field ϕ can be thought of as gauge field. Essentially, we can make a transformation as $\phi^i \rightarrow \alpha \phi^i$ in Eq. (26) with some factor α to obtain

$$\mathcal{S} = \int_0^\beta d\tau \sum_{i,j} c_i^\dagger (\partial_\tau + h_t) c_j + \alpha^2 \phi^i U_{ij} \phi^j + 2\alpha \phi^i U_{ij} n_j,$$

This yields the self-consistent mean field equation

$$\left\langle \frac{\delta \mathcal{S}}{\delta \phi^i} \right\rangle \stackrel{!}{=} 0, \quad \Rightarrow \quad \phi^j = -\frac{2}{\alpha} \langle n_j \rangle.$$

Hence, the self-consistent mean field equation depends on α and is therefore not gauge independent. The problem arises, as we only minimize the action (or energy) of the decoupled, ϕ -dependent Hamiltonian. Instead, we need to minimize the energy of the decoupled Hamiltonian (which can be seen as a choice of a trial Hamiltonian) with respect to the original, quartic Hamiltonian. This can be done in the following way. Let \mathcal{H}_{mf} be (a choice of) a mean field or trial Hamiltonian and \mathcal{H} the original, full Hamiltonian. Then, we can rewrite formally $\mathcal{H} = \mathcal{H}_{\text{mf}} + (\mathcal{H} - \mathcal{H}_{\text{mf}})$. On the level of the free energy it follows the Bogoliubov inequality [44, 45]

$$\mathcal{F} \leq \mathcal{F}_{\text{mf}} + \langle \mathcal{F} - \mathcal{F}_{\text{mf}} \rangle. \quad (30)$$

The right hand side of the inequality is a function of the mean field parameters and we need minimize it with respect to ϕ . In our case, for the full Hamiltonian \mathcal{H} in Eq. (10) and the mean field Hamiltonian in Eq. (23), we obtain the following set of self-consistent mean field equations

$$\phi^0 = -\frac{1}{2} \left(\langle c_i^\dagger c_i \rangle + \langle c_{i+p}^\dagger c_{i+p} \rangle \right), \quad (31)$$

$$\phi^x = -\frac{1}{2} \left(\langle c_i^\dagger c_{i+p} \rangle + \langle c_{i+p}^\dagger c_i \rangle \right), \quad (32)$$

$$\phi^y = -\frac{1}{2} i \left(-\langle c_i^\dagger c_{i+p} \rangle + \langle c_{i+p}^\dagger c_i \rangle \right), \quad (33)$$

$$\phi^z = -\frac{1}{2} \left(\langle c_i^\dagger c_i \rangle - \langle c_{i+p}^\dagger c_{i+p} \rangle \right), \quad (34)$$

or in short hand notation using Pauli matrices

$$\phi^r = -\frac{1}{2} \left\langle c_i^\dagger \sigma_{ij}^r c_j \right\rangle. \quad (35)$$

The real space amplitudes are evaluated as mean over all lattice sites, for instance

$$\langle c_i^\dagger c_{i+p} \rangle = \frac{1}{N_{\text{sites}}} \sum_{\mathbf{k}} e^{i\mathbf{k} \cdot \mathbf{a}_p} \langle c_{\mathbf{k}A}^\dagger c_{\mathbf{k}B} \rangle \quad (36)$$

$$= \frac{1}{N_{\text{sites}}} \sum_{\mathbf{k}} \sum_{\mu', \nu'} e^{i\mathbf{k} \cdot \mathbf{a}_p} \mathcal{M}_{\mathbf{k}A\mu'}^* \mathcal{M}_{\mathbf{k}B\nu'} \langle \gamma_{\mathbf{k}\mu'}^\dagger \gamma_{\mathbf{k}\nu'} \rangle \quad (37)$$

$$= \frac{1}{N_{\text{sites}}} \sum_{\mathbf{k}} \sum_{\lambda} e^{i\mathbf{k} \cdot \mathbf{a}_p} \mathcal{M}_{\mathbf{k}A\lambda}^* \mathcal{M}_{\mathbf{k}B\lambda}. \quad (38)$$

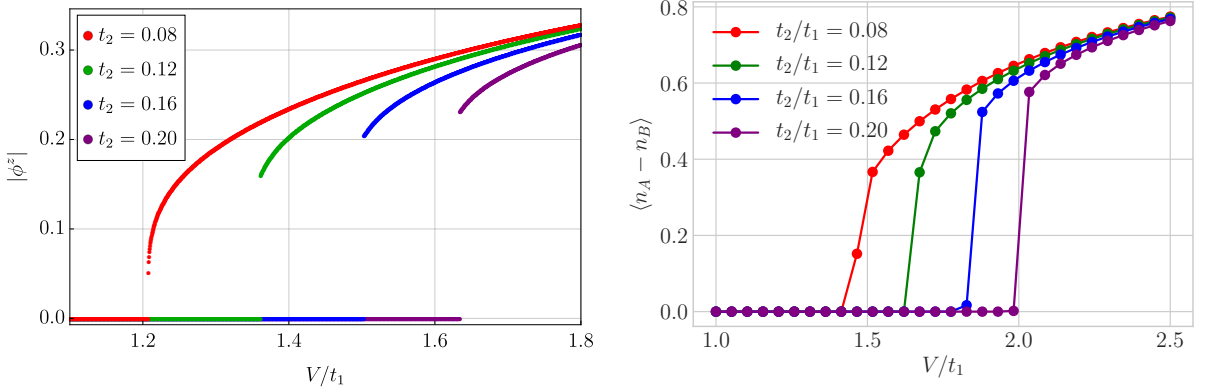


FIG. 6. CDW order parameter from mean field theory (ϕ^z , left) and iDMRG ($L_y = 6$, $\chi = 200$, right) as a function of the interaction strength V/t for different values of the next-nearest neighbor hopping amplitude t_2 . In both cases the smaller t_2 the smaller the jump in the order parameter (in agreement with known results in the literature for $t_2 = 0$ [46]). In the mean field diagram (left), we computed a solution to the self-consistent equations in small incremental steps of $\Delta V = 0.0005$ in order to show clearly the jump in the order parameter for the values of t_2 under investigation.

In the first line, we performed a Fourier transform of the creation and annihilation operators in real space. In the second line, we used $\gamma_{\mathbf{k}} = \mathcal{M}_{\mathbf{k}}^\dagger \psi_{\mathbf{k}}$ where $\mathcal{M}_{\mathbf{k}}$ is a unitary matrix that diagonalizes \mathcal{H}_{mf} . The new spinor basis fulfills $\langle \gamma_{\mathbf{k}\mu'}^\dagger \gamma_{\mathbf{k}\nu'} \rangle = \delta_{\mu'\nu'}$ for occupied states. In Eq. (37), μ' and ν' run over all states, whereas λ in Eq. (38) runs only over occupied states.

ENERGETIC ANALYSIS OF THE PHASE TRANSITION AND THE STOCHASTIC APPROACH

As indicated in the main text, we find at the mean field level a jump of the CDW order parameter ϕ^z at the phase transition for the parameter configuration under investigation. In Fig. 6 (left), we show the CDW order parameter as a function of V for different fixed values of t_2 ranging between $t_2 = 0.08$ and $t_2 = 0.20$. Here, the self-consistent mean equations were solved for increasing V in steps of $\Delta V = 0.0005$ in order to show clearly the jump in the order parameter ϕ^z . The jump becomes smaller the smaller t_2 is. Therefore, at the mean field level, a clear indication of a first order phase transition can only be given when t_2 is sufficiently large, i.e. at the order of t_2 that we consider here. From the Ginzburg-Landau and mean field theoretical point of view a clear analysis of the nature of the mean field analysis for $t_2 < 0.05$ is not possible, the phase transition appears at most rather *weakly* first order when t_2 is close to zero. This observation seems to be in accordance with the literature [46], where a second order phase transition is predicted for vanishing t_2 . From our perspective, the regime of small t_2 seems therefore to be the middle ground between the clear indication of a first order phase transition in the range $t_2 \in (0.08, 0.20)$ and the second order phase transition for vanishing t_2 .

In order to confirm a first order phase transition on the mean field level for sufficiently large t_2 , we compute the total energy of the system. Let $|\Omega_{\text{mf}}\rangle$ denote the mean field ground state which in general depends on the self-consistently obtained field ϕ^r , i.e. $|\Omega_{\text{mf}}\rangle \equiv |\Omega_{\text{mf}}\rangle_{\phi^r}$. Then, we compute the energy of the system via $\mathcal{F}(\phi) = \langle \Omega_{\text{mf}} | \mathcal{H} | \Omega_{\text{mf}} \rangle \equiv \langle \mathcal{H} \rangle$ where $\mathcal{H} = \mathcal{H}_0 + H_V$ is the original Hamiltonian Eq. (10). This calculation involves exactly decomposing the quartic term $n_i n_j = c_i^\dagger c_i c_j^\dagger c_j$ using Wick's theorem [34] as

$$\langle c_i^\dagger c_i c_j^\dagger c_j \rangle = \langle c_i^\dagger c_i \rangle \langle c_j^\dagger c_j \rangle - \langle c_i^\dagger c_j^\dagger \rangle \langle c_i c_j \rangle - \langle c_i^\dagger c_j \rangle \langle c_j^\dagger c_i \rangle. \quad (39)$$

The amplitudes such as $\langle c_i^\dagger c_i \rangle$ are then evaluated similarly to the computation leading to Eq. (38).

Explicitly computing the energy in both phases around the transition shows that the energy curves cross at the transition line, see Fig. 7a) for $t_2 = 0.2$. This indicates a first order transition as the parameter will jump at the transition to the energetically preferable solution.

This can be further confirmed by computing the energy explicitly for small ϕ^z around the saddle-point solution right before the phase transition (also for $t_2 = 0.2$). The curve obtained, Fig. 7b) shows a typical Mexican hat form [34] with co-existing minima. We build a Ginzburg Landau theory, i.e. an expansion of the free energy curve. Finding

	\mathcal{F}_0	α	β	γ
$t_2 = 0.20$ and $V = 1.6250$	-2.0913	0.0402	-1.5045	15.6428
$t_2 = 0.08$ and $V = 1.2074$	-1.8445	0.0001	-0.2575	70.7487
$t_2 = 0.12$ and $V = 1.3610$	-1.8974	0.0010	-1.5419	31.4482
$t_2 = 0.14$ and $V = 1.4250$	-1.9232	0.0212	-1.2630	6.7646

TABLE I. Ginzburg-Landau expansion coefficients (of the polynomial Eq. 40). The coefficients for different values of t_2 are in general difficult to compare since we need for each t_2 to fix some V manually close to the phase transition, and the coefficients are subject to change in magnitude when only moving slightly towards the phase transition or away from it. Comparing signs is however possible, and the configuration at hand ($\alpha > 0$, $\beta < 0$, and $\gamma > 0$) determines a first order phase transition [47].

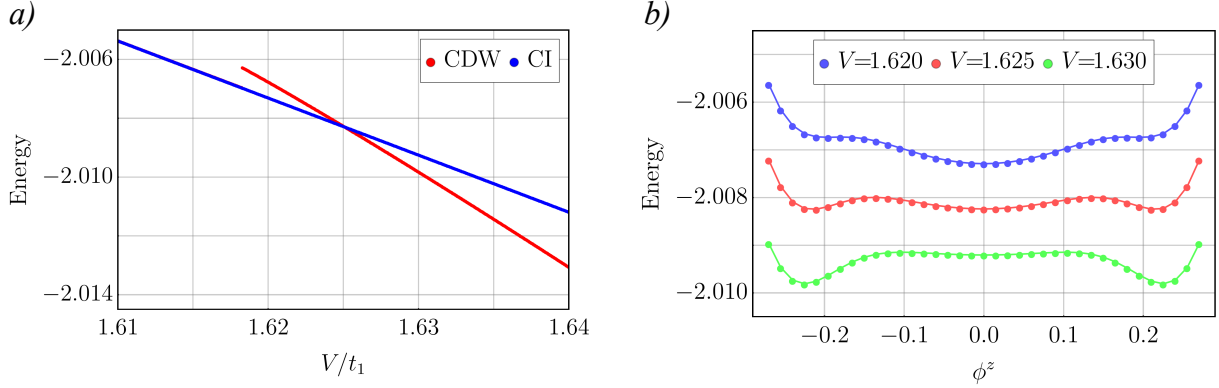


FIG. 7. (color online) (a) Energy of the CI and CDW Mott phases obtained from mean field theory at $t_2 = 0.2$. The curves cut in one point, forcing the CDW order parameter to jump as the system abruptly prefers the change in order to minimize energy. (b) Energy landscape around the mean field solution at $t_2 = 0.2$ in dependence on the CDW order parameter ϕ^z at the phase transition. The coexistence of local minima indicates a first order transition according to Ginzburg-Landau theory.

appropriately relevant terms until the order $(\phi^z)^6$ is a difficult task here because V is large as well as ϕ^x , and therefore we perform this task numerically. The free energy can be approximated by a polynomial of the form

$$\mathcal{F}(\phi^z) = \mathcal{F}_0 + \alpha(\phi^z)^2 + \beta(\phi^z)^4 + \gamma(\phi^z)^6, \quad (40)$$

where the coefficients fulfill in general [47] $\alpha > 0$, $\beta < 0$, and $\gamma > 0$ to ensure the co-existence of local minima and that the free energy is bounded from below. We explicitly fit such a polynomial to the energy computed very close to the phase transition for different values of t_2 . The results are shown in Table I. In general, it is difficult to compare these coefficients for different values of t_2 . For each fixed value of t_2 we need to fix a V that is close to the phase transition in order for the expansion Eq. 40 to be valid. Varying V in the vicinity of the phase transition slightly, i.e. moving either towards the phase transition or away from it, may change the magnitude of the coefficients in Table I. However, we can make a statement on the signs of the coefficients. Since we get across all values of t_2 a consistent configuration of $\alpha > 0$, $\beta < 0$, and $\gamma > 0$, we can confirm the first order nature of the phase transition [47].

Furthermore, note that a plot of the energy landscape around a mean field solution such as Fig. 7b) is an important tool to check the validity of the mean field theory. If relevant mean field parameters are omitted, their weight is not correctly adjusted (the parameters η_r introduced above), or the self-consistent equations have not been such that they minimize the total energy of the system, the energy curve will indeed not show a minimum at the saddle point solution.

Finally, we would like to comment on the stochastic approach to the interacting Chern insulator outlined in the main text from the energetic point of view. Allowing the auxiliary mean field parameters ϕ^r to fluctuate around the saddle point solution changes the energy of the quasi state under consideration. We sample the fields $\phi^{x,y,z}$ and for each configuration we can compute the energy of this quasi state with respect to the wave function $|\Omega\rangle \equiv |\Omega(\phi^x, \phi^y, \phi^z)\rangle$. Repeating this procedure for 10^3 sampled configurations of the $\phi^{x,y,z}$ for each respective V yields Fig. 8. The red line gives the energy of the mean field ground state which is the lowest energy state for each V . Sampling the ϕ^p

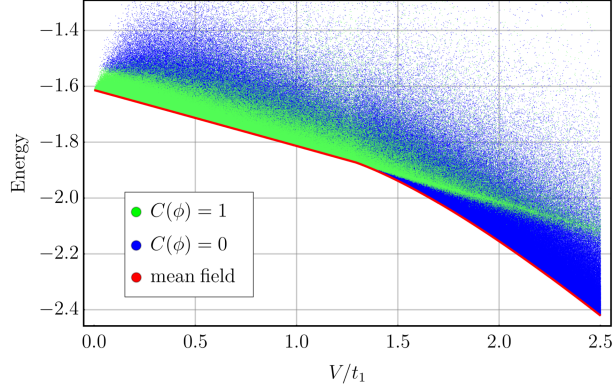


FIG. 8. (color online) Energy of the mean field ground state as function of V (red line). Also shown is the energy distribution of quasi states obtained from sampling $(\phi^x, \phi^y, \phi^z) = \phi$ around the saddle point. This creates quasi-excited states that lie at higher energies than the mean field ground state. Each quasi-state can be attributed a Chern number $C(\phi)$ which will be either one (green) or zero (blue).

fields will result a quasi state at a higher energy. Each quasi state can be associated with a Chern number of either one or zero (depending on ϕ^z). For small V , the mean field ground state (red line) as well as states close to it have Chern number zero. Close to the phase transition, it then becomes more likely to create a state with Chern number zero when moving away from the saddle point. At the phase transition, the ground state acquires Chern number 0 and for further increasing V it becomes more and more unlikely to create an excited state with non-trivial topology.

CIRCULAR DICHROISM OF LIGHT AT THE DIRAC POINTS AND MEASUREMENTS

Here, we show how the information on the topological properties of the system when coupling circularly to light can be obtained at the Dirac points. For this purpose, we address the Bloch sphere geometry. We build a correspondence between transport properties on the lattice and therefore the quantum Hall conductivity and the Bloch sphere description for the light response. We study interaction effects on the Mott transition for the ground state and then propose a protocol to measure the stochastic Chern number C_{st} with applications to the circular dichroism of light.

Poincaré-Bloch sphere formalism

We start from the 2×2 matrix form for the Hamiltonian:

$$\mathcal{H}_0(\mathbf{k}) = \begin{pmatrix} \gamma(\mathbf{k}) & -g(\mathbf{k}) \\ -g^*(\mathbf{k}) & -\gamma(\mathbf{k}) \end{pmatrix}, \quad (41)$$

which is the pure Haldane model with no mean field parameters ϕ^r . Its energy eigenvalues read

$$(\epsilon_u^{\mathbf{k}}, \epsilon_l^{\mathbf{k}}) = \pm \sqrt{\gamma^2(\mathbf{k}) + |g(\mathbf{k})|^2} \equiv \pm \epsilon^{\mathbf{k}}, \quad (42)$$

where the positive sign refers to the upper band and the minus sign to the lower band. In analogy with a spin-1/2 Hamiltonian described by a polar angle θ and azimuthal angle φ we can parametrize the Hamiltonian as

$$\frac{\gamma(\mathbf{k})}{\epsilon^{\mathbf{k}}} = \cos \theta, \quad -\frac{g^*(\mathbf{k})}{\epsilon^{\mathbf{k}}} = e^{i\varphi} \sin \theta. \quad (43)$$

From quantum mechanics and the definition of eigenstates of a spin-1/2 particle, the two eigenstates $|u\rangle$ and $|l\rangle$ referring to upper and lowest bands respectively, take the form

$$|u\rangle = e^{-i\varphi/2} \cos(\theta/2) |a\rangle + e^{i\varphi/2} \sin(\theta/2) |b\rangle, \quad (44)$$

$$|l\rangle = -e^{-i\varphi/2} \sin(\theta/2) |a\rangle + e^{i\varphi/2} \cos(\theta/2) |b\rangle. \quad (45)$$

Here, the kets $|a\rangle$ and $|b\rangle$ refer to the states acting on sublattice A and sublattice B , respectively, for a given wavevector. At the two Dirac points, we have $g(\mathbf{K}/\mathbf{K}') = 0$ and $\epsilon_u(\mathbf{K}) = +m/2 = -\epsilon_u(\mathbf{K}')$. Similarly, we have the important mass identifications for the lower band $\epsilon_l(\mathbf{K}) = -m/2 = -\epsilon_l(\mathbf{K}')$.

For the light-matter coupling, here we use a formulation written in terms of the vector potential. Using the spin Pauli matrix representation then this is analogous to the modification in the Dirac Hamiltonian $i(\mathbf{p} + \mathbf{A}e/c) \cdot \boldsymbol{\sigma}$ where we set e and c to unity. In the circular basis, the vector potential is defined as $\mathbf{A} = A_0 e^{-i\omega t} (\mathbf{e}_x \mp i\mathbf{e}_y)$ where \mathbf{e}_x and \mathbf{e}_y are unit vectors associated with the x and y directions. The signs in $(\mathbf{e}_x \mp i\mathbf{e}_y)$ refer to right-handed (+) and left-handed (-) polarizations respectively. With such definitions, we obtain the light-matter Hamiltonian:

$$\delta\mathcal{H}_{\pm} = A_0 e^{\pm i\omega t} |a\rangle\langle b| + h.c. \quad (46)$$

This is also equivalent to

$$\delta\mathcal{H}_{\pm} = A_0 \cos(\omega t) (|a\rangle\langle b| + |b\rangle\langle a|) \mp \frac{A_0}{i} \sin(\omega t) (|a\rangle\langle b| - |b\rangle\langle a|). \quad (47)$$

To obtain these equations, we have considered the real parts of the vector potential components $A_x(t)$ and $A_y(t)$ to ensure that the Hamiltonian is hermitian. The speed at the Dirac points is absorbed in A_0 within this notation for $t_2 < 0.2t_1$. Within this formulation, changing the sense of circulation for light is equivalent to change $\omega \rightarrow -\omega$, and the subscript \pm refers to a Jones polarization of light. We can then rewrite $\delta\mathcal{H}_{\pm}$ in the band basis (which diagonalizes the Hamiltonian), and we obtain two classes of terms which can be then studied by mapping the Brillouin zone onto the Bloch sphere

$$\delta\mathcal{H}_{\pm} = A_0 \sin(\theta) \cos(\omega t \pm \varphi) (|u\rangle\langle u| - |l\rangle\langle l|) + A_0 (e^{\pm i\omega t} e^{i\varphi} \cos^2(\theta/2) - \sin^2(\theta/2) e^{\mp i\omega t} e^{-i\varphi}) |u\rangle\langle l| + h.c.. \quad (48)$$

The first term produces a time-dependent shift of the chemical potential in the original Haldane model, and therefore to ensure the validity of the topological phase, we require that A_0 is small such that the chemical potential is in the band gap. Now, we can apply Fermi's golden rule argument for the inter-band transitions.

The transition rates $\Gamma_+(\mathbf{k})$ and $\Gamma_-(\mathbf{k})$ are defined such that the two terms in $\delta\mathcal{H}_{\pm}$ proportional to $|u\rangle\langle l|$, for a given light polarization, correspond to an absorption of a light quantum with energy $\hbar\omega$ and $-\hbar\omega$ respectively and we assume a sampling on frequencies from $-\infty$ to $+\infty$ as realized below to define the topological response.

For the + polarization, then:

$$\Gamma_+(\mathbf{k}) = \frac{2\pi}{\hbar} |\langle u | \delta\mathcal{H}_{\pm} | l \rangle|^2 \delta(\epsilon_u^{\mathbf{k}} - \epsilon_l^{\mathbf{k}} - \hbar\omega). \quad (49)$$

This results in:

$$\Gamma_+(\mathbf{k}) = \frac{2\pi}{\hbar} A_0^2 \frac{1}{2} (1 + \cos^2(\theta)) \delta(\epsilon_u^{\mathbf{k}} - \epsilon_l^{\mathbf{k}} - \hbar\omega), \quad (50)$$

corresponding to a rotating wave approximation. The time-dependent corrections average to zero if one considers a time-Floquet average of the rates or if one goes to the rotating-wave basis. The energy conservation can be equivalently rewritten in terms of a given band $\delta(\epsilon_u^{\mathbf{k}} - \epsilon_l^{\mathbf{k}} - \hbar\omega) = \delta(-\epsilon_l^{\mathbf{k}} - \hbar\omega/2) = \delta(\epsilon_u^{\mathbf{k}} - \hbar\omega/2)$.

The important point within this simple argument is that if we change the polarization of light, only the sign of $\hbar\omega$ is changing in the energetic conservation law since by definition $\mathcal{H}_+(\omega) = \mathcal{H}_-(-\omega)$. Therefore,

$$\Gamma_-(\mathbf{k}) = \frac{2\pi}{\hbar} A_0^2 \frac{1}{2} (1 + \cos^2(\theta)) \delta(\epsilon_u^{\mathbf{k}} - \epsilon_l^{\mathbf{k}} + \hbar\omega). \quad (51)$$

Application of Stokes Theorem to Circular Dichroism of Light

Now, we relate the light responses with topological properties of the spin-1/2 particle applying the Stokes theorem as in Ref. [31], with the introduction of smooth fields. The Chern number is defined in terms of the Berry curvature as

$$C = -\frac{1}{2\pi} \int_{S^2} \nabla \times \mathbf{A} d^2 \mathbf{n}, \quad (52)$$

where $\mathbf{A} = \langle \psi | i\nabla | \psi \rangle$ with $|\psi\rangle = |l\rangle$ or $|u\rangle$ and $\nabla = (\partial/\partial\varphi, \partial/\partial\theta)$. We decompose the hemisphere into a north and south hemispheres such that

$$C = -\frac{1}{2\pi} \int_{north} \nabla \times \mathbf{A}_N d^2\mathbf{n} - \frac{1}{2\pi} \int_{south} \nabla \times \mathbf{A}_S d^2\mathbf{n}. \quad (53)$$

$$C = -\frac{1}{2\pi} \int_0^{2\pi} d\varphi A'_{N\varphi}(\varphi, \theta_c) + \frac{1}{2\pi} \int_0^{2\pi} d\varphi A'_{S\varphi}(\varphi, \theta_c) \quad (54)$$

such that θ_c refers to the boundary. Here, to make link with the circular dichroism of light we will set $\theta_c = \pi/2$. The smooth fields are defined as

$$A'_{N\varphi}(\varphi, \theta) = A_{N\varphi}(\varphi, \theta_c) - A_\varphi(0) \quad (55)$$

$$A'_{S\varphi}(\varphi, \theta) = A_{S\varphi}(\varphi, \theta_c) - A_\varphi(\pi) \quad (56)$$

with $\text{curl} \mathbf{A}' = \text{curl} \mathbf{A}$. The smooth fields are uniquely defined on the surface of the sphere, where $A_\varphi(0) = \lim_{\theta \rightarrow 0} A(\varphi, \theta)$ and $A_\varphi(\pi) = \lim_{\theta \rightarrow \pi} A(\varphi, \theta)$. The poles require special care because the φ angle is not uniquely defined. The smooth fields satisfy $A'_{N\varphi}(\varphi, \theta) \rightarrow 0$ when $\theta \rightarrow 0$ and $A'_{S\varphi}(\varphi, \theta) \rightarrow 0$ when $\theta \rightarrow \pi$.

For the lowest band $|l\rangle$, we have

$$A_\varphi(\varphi, \theta) = -\frac{\cos \theta}{2}. \quad (57)$$

At the equator, $A_\varphi(\varphi, \pi/2) = 0 = A_{N\varphi}(\varphi, \pi/2) = A_{S\varphi}(\varphi, \pi/2)$, and

$$A'_{N\varphi}(\varphi, \theta = \pi/2) = \frac{1}{2} = -A'_{S\varphi}(\varphi, \theta = \pi/2). \quad (58)$$

The topological number has then two simple interpretations

$$C = A_\varphi(0) - A_\varphi(\pi) = -1 \quad (59)$$

and

$$C = A'_{S\varphi}(\varphi, \theta = \pi/2) - A'_{N\varphi}(\varphi, \theta = \pi/2) = -1. \quad (60)$$

In addition, we have the identities

$$A'_{N\varphi}(\varphi, \theta) = \frac{1}{2}(-\cos \theta + 1) = \sin^2 \frac{\theta}{2} \quad (61)$$

and

$$A'_{S\varphi}(\varphi, \theta) = \frac{1}{2}(-\cos \theta - 1) = -\cos^2 \frac{\theta}{2}. \quad (62)$$

This formula shows that one can then perform closed circles with $\varphi \rightarrow \varphi + 2\pi$ for any angle $\theta \in]0; \pi[$ and measure the Chern number. This is in accordance with the Stokes theorem, since θ_c can be defined arbitrarily from 0^- to π^- .

This equatorial plane representation seems justified since we introduce the vector potential with (real) components in the XY plane $A_x = A_0 \cos(\omega t)$ and $A_y = \mp A_0 \sin(\omega t)$ such that the azimuthal angle can be redefined as $\varphi = \varphi_0 \mp \omega t$ for the \pm polarizations of light. Averaging on angles φ is similar to perform a Floquet average on a time period. A closed path involving a change of the angle $\varphi \in [0; 2\pi]$ in the equatorial plane corresponds to perform a similar circular closed path in the wavevector space. This situation is similar to the nuclear magnetic resonance where we obtain a signal $\frac{1}{2} \sin^2 \theta$ when performing a Floquet average of the signal.

At the equator, for $\theta = \pi/2$, to reveal the topological properties in the light response we use the identity

$$\sin \theta = 2 \sin(\theta/2) \cos(\theta/2) = \sqrt{2} \sin(\theta/2). \quad (63)$$

Then, we re-write

$$\Gamma_+(\mathbf{k}, \omega) = \frac{2\pi}{\hbar} A_0^2 (1 - A'_{N\varphi}(\varphi, \theta)) \delta(-\epsilon_l^{\mathbf{k}} - \hbar\omega/2) \quad (64)$$

and

$$\Gamma_+(\mathbf{k}, \omega) = \frac{2\pi}{\hbar} A_0^2 (-A'_{S\varphi}(\varphi, \theta)) \delta(-\epsilon_l^{\mathbf{k}} - \hbar\omega/2). \quad (65)$$

This term then probes the first circle at the equator in the definition of C

$$\int_{-\infty}^{+\infty} d\omega \frac{1}{2\pi} \int_{2\pi}^0 d\varphi \Gamma_+(\theta = \pi/2, \varphi, \omega) = \frac{2\pi}{\hbar} A_0^2 A'_{S\varphi}(\theta = \pi/2). \quad (66)$$

For the + light polarization, the angle φ goes from 2π to 0 since $\varphi = \varphi_0 - \omega t$. For the - light polarization,

$$\Gamma_-(\mathbf{k}, \omega) = \frac{2\pi}{\hbar} A_0^2 (-A'_{S\varphi}(\varphi, \theta)) \delta(\epsilon_l^{\mathbf{k}} - \hbar\omega/2). \quad (67)$$

and under the parity transformation, this is equivalent to

$$\Gamma_-(-\mathbf{k}, \omega) = \frac{2\pi}{\hbar} A_0^2 A'_{N\varphi}(\varphi, \theta) \delta(\epsilon_l^{-\mathbf{k}} - \hbar\omega/2). \quad (68)$$

At the equator $\epsilon_l^{-\mathbf{k}} = \epsilon_l^{\mathbf{k}}$. Then, we obtain:

$$\int_{-\infty}^{+\infty} d\omega \frac{1}{2\pi} \int_{2\pi}^0 d\varphi (\Gamma_+(\theta = \pi/2, \varphi, \omega) + \Gamma_-(\pi - \theta = \pi/2, -\varphi, \omega)) = \frac{2\pi}{\hbar^2} A_0^2 (A'_{S\varphi}(\theta = \pi/2) - A'_{N\varphi}(\theta = \pi/2)). \quad (69)$$

If we change + into - and also change $\varphi \rightarrow -\varphi$, the two signals are additive. We also have

$$\int_{-\infty}^{+\infty} d\omega \frac{1}{2\pi} \int_{2\pi}^0 d\varphi (\Gamma_+(\pi - \theta = \pi/2, \varphi, \omega) + \Gamma_-(\theta = \pi/2, -\varphi, \omega)) = \frac{2\pi}{\hbar^2} A_0^2 (A'_{S\varphi}(\theta = \pi/2) - A'_{N\varphi}(\theta = \pi/2)). \quad (70)$$

The right-hand side is invariant under a change of θ and can be equivalently re-written as

$$\frac{2\pi}{\hbar^2} A_0^2 (A'_{S\varphi}(\theta) - A'_{N\varphi}(\theta)) = \frac{2\pi}{\hbar^2} A_0^2 (A_\varphi(0) - A_\varphi(\pi)). \quad (71)$$

For $\theta \rightarrow 0$, from Eqs. (69) and (70) then we find

$$\int_0^{+\infty} d\omega \frac{1}{2\pi} \oint dl \sum_{\mathbf{k}=\mathbf{K}, \mathbf{K}'} \frac{(\Gamma_+(\mathbf{k}, \omega) - \Gamma_-(-\mathbf{k}, \omega))}{2} = \frac{2\pi}{\hbar^2} A_0^2 C. \quad (72)$$

The integration on frequencies can be equivalently re-written as an integration from 0 to $+\infty$. We introduce a vector representation $\mathbf{\Gamma}_+(\varphi) = \Gamma_+(\varphi) \nabla \varphi$ such that $\mathbf{\Gamma}_-(-\varphi) = -\Gamma_-(-\varphi) \nabla \varphi$. See also discussion below Eq. (79) for another definition of the light responses related to the definitions in the article. It's important to note that here C measures topological properties of the lowest occupied band and therefore of the ground state.

Relation to Transport Properties on the Lattice and Interaction Effects

Now, we show a relation between spin observables and the formula (3) in the article making a link with transport properties. The current density at site i is related to $j_i \propto d(c_{iA}^\dagger c_{iA} - c_{iB}^\dagger c_{iB})/dt$. From Eq. (46), we probe the current induced by light for a particle moving from site A onto a nearest-neighbor site B in a unit cell i of the system, i.e. the variation of particles on a given sub-lattice and holes in the other sub-lattice (we assume fermions). We study the response on a given bond formed by two nearest-neighbors. As defined in our model, the light response moves a particle from site A to B . To make the link with the spin observables in the wave-vector space, we make an average of the current density in real space, referring to $\bar{j} = 1/N \sum_{i=1}^N j_i$ and N refers to the number of cells in the system.

We realize a mean on all the bonds of the lattice oriented in the same direction. Then, we relate the light response and the spin observable in the wave-vector space as

$$\bar{j} = \frac{1}{N} \sum_{\mathbf{k}} \frac{d}{dt} \sigma^z(\mathbf{k}). \quad (73)$$

Within our definitions, $\sigma^z = \sigma^z(\mathbf{k})$ is the Pauli matrix with eigenvalue +1 when projecting on $|a(\mathbf{k})\rangle$ and eigenvalue $|- \rangle$ when projecting on $|b(\mathbf{k})\rangle$. In the many-body representation, this is also equivalent to $\sigma^z(\mathbf{k}) = c_{\mathbf{k}A}^\dagger c_{\mathbf{k}A} - c_{\mathbf{k}B}^\dagger c_{\mathbf{k}B}$. Writing the equations of motion for the spin observables, we find

$$\frac{d}{dt} \sigma^z(\mathbf{k}) = \frac{2}{\hbar} \left((p_x + A_x) \frac{\partial \mathcal{H}}{\partial p_y} - 2(p_y + A_y) \frac{\partial \mathcal{H}}{\partial p_x} \right). \quad (74)$$

We have the relations $p_x = \hbar k_x$ and $p_y = \hbar k_y$ and with our notations p_x and p_y go to zero at the Dirac points. If we build a Golden rule argument in this current density, to second order in A_0 , all wave-vectors equally contribute (similarly as if p_x and p_y go to zero) and then

$$\bar{j}(\mathbf{k}) = \frac{2}{\hbar} \left(A_x \frac{\partial \mathcal{H}}{\partial p_y} - A_y \frac{\partial \mathcal{H}}{\partial p_x} \right). \quad (75)$$

This justifies why we can reproduce the same response for the present Dirac Hamiltonian when considering the \mathbf{K} and \mathbf{K}' only. The current density here is written in terms of the Pauli matrix σ^z and the commutation relations for the spin-1/2 then allows us to bridge with the transport properties.

Now, to make an identification with equation (3) in the article we can include the forms of A_x and A_y for the two polarizations and therefore we obtain

$$\bar{j}(\mathbf{k}) = \bar{j}(\mathbf{k}, t) = \frac{2}{\hbar} A_0 \left(\cos(\omega t) \frac{\partial \mathcal{H}}{\partial p_y} \pm \sin(\omega t) \frac{\partial \mathcal{H}}{\partial p_x} \right). \quad (76)$$

This is equivalent to

$$\bar{j}(\mathbf{k}) = \frac{1}{\hbar} A_0 e^{i\omega t} \left(\frac{\partial \mathcal{H}}{\partial p_y} \pm \frac{1}{i} \frac{\partial \mathcal{H}}{\partial p_x} \right) + \frac{1}{\hbar} A_0 e^{-i\omega t} \left(\frac{\partial \mathcal{H}}{\partial p_y} \mp \frac{1}{i} \frac{\partial \mathcal{H}}{\partial p_x} \right) = \frac{1}{\hbar} A_0 e^{i\omega t} \left(\frac{\partial \mathcal{H}}{\partial p_y} \pm \frac{1}{i} \frac{\partial \mathcal{H}}{\partial p_x} \right) + h.c. \quad (77)$$

Using Eq. (46), this is also equivalent to

$$\bar{j}(\mathbf{k}) = \pm \frac{i}{\hbar} A_0 e^{i\omega t} (\sigma^x \pm i\sigma^y) + h.c. = \pm \frac{i}{\hbar} \mathcal{H}_{\pm}(\mathbf{k}) + h.c. \quad (78)$$

Here, $\sigma^x \pm i\sigma^y$ refers to the raising and lowering operators. One can then equally perform the Fermi Golden rule with the current density \bar{j} , which then gives

$$\Gamma_{\pm} = \frac{2\pi}{\hbar} \sum_{\mathbf{k}=\mathbf{K},\mathbf{K}'} \frac{A_0^2}{\hbar^2} \left| \left\langle u \left| \left(\frac{\partial \mathcal{H}}{\partial p_y} \pm \frac{1}{i} \frac{\partial \mathcal{H}}{\partial p_x} \right) \right| l \right\rangle \right|^2 \delta(\epsilon_u^{\mathbf{k}} - \epsilon_l^{\mathbf{k}} - \hbar\omega). \quad (79)$$

One Dirac point only contributes for a given light polarization when $\omega > 0$. The light responses are the ones in the article where we use the electric field strength E through $A_0 = E/\omega$ and the additional $(1/\hbar)^2$ factor comes from the definition of the current density. A similar formula was previously derived in Ref. [29], but including the summation on all the wave-vectors in the first Brillouin zone. In that paper, the authors also show the relation between this formula and the quantum Hall conductivity with a different approach. We deduce that the Bloch sphere is useful to show why one can just perform a sum at the two Dirac points and reproduce the quantum Hall conductivity. In Eq. (79), the left and right-handed light polarizations are related through the modification $p_x \rightarrow -p_x$ implying to modify the reciprocal lattice vectors with a minus sign in Fig 5 and similarly for the sum on wave-vectors. This justifies why in Eq. (4) of the Letter, Γ_+ and Γ_- enter with a relative minus sign.

It's important to emphasize that here we probe ground state properties because the result in Eq. (72) is equivalent to perform an average on a time Floquet period at the equator (in the limit of A_0 small). This correspondence then shows why the topological number occurs in the circular dichroism of light. One can equivalently introduce the velocity components as $dx/dt = \dot{x} = i\sigma_x$ and $dy/dt = \dot{y} = i\sigma_y$. Therefore, $\bar{j}(\mathbf{k}) = \pm i(A_0/\hbar) e^{i\omega t} (-i\dot{x} \pm i\dot{y}) = \pm (A_0/\hbar) e^{i\omega t} (\dot{x} \pm i\dot{y})$.

The velocity components are in agreement with the definition of the circular basis in terms of the vectors \mathbf{e}_x and $\mp i\mathbf{e}_y$ such that $\mathbf{r} = (x, \pm iy)$ in this coordinate system such that we also have $\mathbf{r} = x\mathbf{e}_x + y\mathbf{e}_y$ in the plane.

In our description of the interactions, the V term is re-written self-consistently in terms of the stochastic ϕ^x , ϕ^y and ϕ^z variables. For the ground-state properties, we can then show that the topological properties are not modified and a jump of the Chern number should be observed at the Mott transition both with the quantum Hall conductivity and with the light response. More precisely, the stochastic variables ϕ^x and ϕ^y describing the particle-hole channel commute with σ^z and $\langle \phi^z \rangle = 0$ for the ground state properties in the topological phase (since the system, on average, has the same probability to be on $|a\rangle$ or on $|b\rangle$). The arguments shown above leading to Eq. (79) then ensure that the same topological response should be observed for ground-state properties in the topological phase through the light response or through the quantum Hall conductivity, as shown in the article. In the Mott phase, the charge density-wave order becomes finite in real-space implying here a jump in $\langle j_i \rangle$ or $\langle \bar{j} \rangle$. In agreement with numerical calculations, the Chern number C_{gs} jumps to 0 since $\langle \sigma_i^z \rangle$ becomes polarized (fixed) in real space and does not depend on time.

Protocols in time revealing C_{st}

Here, we describe the measurement of the stochastic Chern number C_{st} on the sphere at zero temperature in relation with Eq. (59) which relates the north to south poles. Then, from Stokes theorem discussed above we will adapt the argument for the circular dichroism of light. We define a path on the sphere where we drive changing the polar angle linearly with time, $\theta = vt$ [31].

From the chain rule

$$\bar{j} = \frac{v}{N} \sum_{\mathbf{k}} \frac{\partial}{\partial \theta} \sigma^z. \quad (80)$$

When we follow a path from north to south pole, we fix $\varphi = 0$ and $\sum_{\mathbf{k}} \rightarrow \int_0^\pi d\theta$. Then,

$$\frac{\langle \bar{j} \rangle}{vn} = \frac{(\langle \sigma^z(\theta = \pi) \rangle - \langle \sigma^z(0) \rangle)}{2} = -C. \quad (81)$$

It is interesting to relate $\langle \bar{j} \rangle = \langle l | \bar{j} | l \rangle$ with an effective current density of the form $\langle q^* \rangle nv$ in real space on the lattice. Here, the speed corresponds to the speed of the driving on the sphere, the density is $n = 2/N$ since we probe half of the \mathbf{k} values and the average pumped charge $\langle q^* \rangle = (\langle \sigma^z(\theta = \pi) \rangle - \langle \sigma^z(0) \rangle)/2$ is equal to $-C$ for the Haldane model [31]. When we increase the speed the system has a chance to pass from the lower $|l\rangle$ to the upper band $|u\rangle$ in relation with Landau-Zener energy band crossing effects, which should then reduce the value of $\langle q^* \rangle$. For a finite speed in the protocol, the mapping with the Landau-Zener model is applicable close to the south pole if we identify $vt = \pi + \tilde{v}t$. In that case, we identify the effective Hamiltonian from Eq. (41) and including the effect of the stochastic field ϕ^z :

$$\mathcal{H}_{eff} \approx (\epsilon_l(\mathbf{K}') + 3V\phi^z)\sigma^z + v\tilde{v}\epsilon_l(\mathbf{K}')\sigma^x. \quad (82)$$

At the south pole or \mathbf{K}' Dirac point, within our definitions the spin is in the $|a\rangle$ state with energy $\epsilon_l(\mathbf{K}') \sim -|m|/2$. We can adjust properly the spinor definition of $|a\rangle$ to satisfy this energy requirement at the south pole for a given sign of m . For $V = 0$, one can measure the Landau-Zener effect when defining [31]

$$\tilde{C} = \frac{1}{2} (\langle \sigma^z(\theta = 2\pi) \rangle - \langle \sigma^z(\theta = \pi) \rangle). \quad (83)$$

Indeed, when going back up to the north pole irreversibility effects take place as a result of band crossing effects close to the south pole and $\tilde{C} \neq C$ when v is finite. More precisely, adapting the Landau-Zener protocol for our situation, then we find $\langle \sigma^z(\theta = \pi) \rangle = +1$ and $\langle \sigma^z(\theta = 2\pi) \rangle = -1 + \mathcal{O}(e^{-m^2/(\hbar v \epsilon_l(\mathbf{K}'))})$. Here, in the Landau-Zener argument, we estimate that $\mathcal{O}(e^{-m^2/(\hbar v \epsilon_l(\mathbf{K}'))})$ corresponds to occupying the upper band at the equator where eigenstates are oriented in the σ^x direction. Going back to the north pole, the probability to occupy the lowest band is equal to $1 - \mathcal{O}(e^{-m^2/(\hbar v \epsilon_l(\mathbf{K}'))})$. Therefore [31],

$$\tilde{C} = C + \mathcal{O}(e^{-m^2/(\hbar v |\epsilon_l(\mathbf{K}')|)}), \quad (84)$$

where here $C = -1$. For the lowest band, the situation is similar as if the pumped charge from south to north pole is modified as $\langle q^* \rangle = -\tilde{C} = 1 - \mathcal{O}(e^{-m^2/(\hbar v |\epsilon_l(\mathbf{K}')|)})$.

In the presence of interactions, the key ingredient in this protocol is that we start in a ‘non-equilibrium’ situation where $\langle n_A - n_B \rangle \sim 1$ due to the magnetic field. Starting at the south pole, this is equivalent as if all the bonds of the lattice would be polarized in the $|a\rangle$ direction implying $\phi^z \sim 1$. Therefore, assuming that $V > |m|/6 = |\epsilon_l(\mathbf{K}')|/3$, we can fulfill the prerequisite $\phi^z > \phi_c^z$, where $\phi_c^z = |m|/6V$ is defined in the Letter, which might allow us to probe additional interactions’ effects in Eq. (84). (For $V < |m|/6$, the situation would be then identical to the case $V = 0$. The case $V = |m|/6$ is indeed special as we observe through \mathcal{H}_{eff} leading to a gap closing at the south pole.) The energy increases at the south pole by an amount $\sim 3V$ due to interaction effects. At the north pole, in this protocol, we measure the pumped charge and therefore for the system this is equivalent as if $3V\phi^z\sigma^z = -3V\sigma^z(\theta = 2\pi) = 3V\langle q^* \rangle$ with the averaged pumped charge $\langle q^* \rangle$ in the lowest band. Now, we show that through interaction effects at the south pole, \tilde{C} is related to C_{st} in the Letter. The effect of interactions in \mathcal{H}_{eff} is equivalent to change $\epsilon_l(\mathbf{K}') \rightarrow \epsilon_l(\mathbf{K}') - 3V$ such that the mass m would stay unchanged and from Eq. (84), we then have

$$\tilde{C} = C + \mathcal{O}(e^{-m^2/(\hbar v|\epsilon_l(\mathbf{K}')-3V|)}). \quad (85)$$

If we assume now that $V \gg |\epsilon_l(\mathbf{K}')|/3$, this formula may be further simplified and we observe an identification between $|\tilde{C}|$ in this protocol and the estimation of C_{st} defined below Equation (6) in the article, with an effective temperature $k_B T_{eff} = \sqrt{\hbar v 3V}$. For any infinitesimally small speed v , the Landau-Zener effect promoting the production of a particle-hole pair is dominated by interaction effects and the result becomes similar as if we set $\phi^z \sim \phi_c^z$ within the stochastic approach at equilibrium (revealing C_{st}). Note that in the formula, page 4 top right of the Letter, the factor 2 multiplying $P(|\phi^z| \sim |\phi_c^z|)$ occurs because when sampling the ϕ^z variable we probe corrections either at $\phi^z \sim \phi_c^z$ or at $-\phi^z \sim -\phi_c^z$. Here, we can precisely probe this factor 2 in the protocol, by changing the direction of the magnetic field corresponding then to modify $m \rightarrow -m$. The spin at the south pole is now polarized in the $\sigma_z \sim -1$ state and we have $\phi^z \rightarrow -\phi^z$ with $\epsilon_l(\mathbf{K}') \rightarrow -\epsilon_l(\mathbf{K}')$ in \mathcal{H}_{eff} . The same arguments would give the same value of $|\tilde{C}| = |C| - \mathcal{O}(e^{-m^2/(\hbar v|\epsilon_l(\mathbf{K}')-3V|)})$. Adding the corrections from the two protocols associated to the value $|C|$, then we probe the factor 2. The stochastic variable ϕ^z is indeed defined on the whole real axis, justifying this factor 2.

From the Stokes theorem shown in the preceding section, it is then suggestive that similar arguments can be adapted for the circular dichroism of light with a precise time-dependent protocol at the equator. If we take the present formalism with $\theta = vt$ on the Bloch sphere, in the azimuthal plane, Eq. (82) is equivalent to have an additional vector potential component $\tilde{A}_x = A_0 \sin(vt) \cos \varphi$ and $\tilde{A}_y = A_0 \sin(vt) \sin \varphi$ with $\varphi = \omega t$ and $v \ll \omega$ such that $\sin(vt) \sim (vt)$ in a time-Floquet period $t \in [0; 2\pi/\omega]$. Therefore, suppose we start from Eq. (78) and adjust A_0 by $A_0(1 + vt)$. This argument then supports the fact that the light response will also measure $|\tilde{C}| \sim C_{st}$ in this case. In the presence of the additional term $A_0 vt$, the particle has a finite probability to leak to the upper band during the Floquet time period $t \in [0; 2\pi/\omega]$ and therefore this reduces the probability to occupy the lowest energy band. Through the stochastic approach, Eq. (85) is yet applicable in this case. We deduce that this protocol allows us to reveal the ensemble-averaged stochastic light responses shown in Fig. 3d) of the Letter. Including a small time-dependent perturbation $A_0 vt$ reveals interaction effects in the Landau-Zener mechanism, i.e. in the process of creating a particle-hole pair. This term then turns the ‘virtual’ production of a particle-hole pair setting $\phi^z \sim \phi_c^z$ within the stochastic approach into a measurable production of a particle-hole pair mediated by the Landau-Zener mechanism. It’s also important to emphasize that interaction effects can be observed as long as $V > |m|/6$.

We now discuss temperature effects and the finite temperature Hall conductivity.

FINITE TEMPERATURE VERSION OF THE TOPOLOGICAL INDEX

In Ref. [32], a finite temperature version of the Hall conductivity was introduced as

$$\sigma_{xy}(k_B T)h/e^2 = \sum_{\alpha \in \{u, l\}} \int_{\mathbf{k} \in \text{BZ}} d\mathbf{k} p^{\mathbf{k}}(k_B T) F_{x,y}^{\alpha}(\mathbf{k}) \quad (86)$$

with the Fermi distribution Fermi distribution $p^{\mathbf{k}}(\epsilon_{u,l}^{\mathbf{k}}) = (\exp(\epsilon_{u,l}^{\mathbf{k}}/k_B T) + 1)^{-1}$. Here, the factor $p^{\mathbf{k}}$ effectively mixes upper and lower band states. Hence, Eq. (86) will yield a topological index one for zero temperature and a many-body topological index that approaches zero in the limit of large temperatures, see Fig. 9. Furthermore note, that Eq. (86) takes heating effects from the bulk into account such that even in a zero-temperature trivial phase, Eq. (86) will yield a many-body Hall conductivity larger than zero for $T > 0$ [32].

For the circular dichroism of light, we can produce a similar finite temperature version as in Ref. [32] such that the

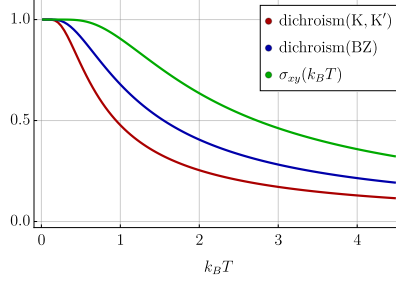


FIG. 9. (color online) Finite temperature version of the topological index. Green: definition from Ref. [32] as in Eq. (86). Blue: based on Eq. (87). Red: Circular dichroism of light as presented in Ref. [29], with a momentum-integral over the entire Brillouin zone.

finite temperature version of Eq. (72) reads

$$\int_0^{+\infty} d\omega \sum_{\mathbf{k}=\mathbf{K}, \mathbf{K}'} \sum_{\alpha=l \rightarrow u, u \rightarrow l} \frac{p^{\mathbf{k}} \Gamma_{\alpha}^{+}(\mathbf{k}) - p^{\mathbf{k}} \Gamma_{\alpha}^{-}(\mathbf{k})}{2}. \quad (87)$$

Note that Eq. (86) and Eq. (87) yield in principle the same result, however the finite temperature topological index scales slightly differently with $k_B T$. Also a finite temperature version of the circular dichroism that integrates over the entire Brillouin zone shows a different scaling behavior, see Fig. 9.

Taking into account that at very low temperatures

$$(1 + \exp(-\epsilon^{\mathbf{k}}/k_B T))^{-1} \approx 1 \quad \text{and} \quad (1 + \exp(\epsilon^{\mathbf{k}}/k_B T))^{-1} \approx \exp(-\epsilon^{\mathbf{k}}/k_B T), \quad (88)$$

then we obtain that in the formula above, C would acquire $\mathcal{O}(e^{-|m|/k_B T})$ corrections in agreement with the Arrhenius law for the distribution of particle-hole pairs in the upper band at finite temperature. We then check that combined interaction and drive effects studied in the preceding section have a similar effect as heating in the sense that they produce an effective temperature effect scaling as \sqrt{V} .

DMRG COMPUTATIONAL DETAILS

In this section we give further details of our infinite density matrix renormalization group results (iDMRG). All our results are computed using the open source package TEPY [36], which implements the iDMRG algorithm [48] in the language of matrix-product states. The bond dimension χ sets the maximum linear dimension of the matrices that are stored to represent a given ground-state, and determines the accuracy of the method. For a given χ the variational algorithm determines the ground-state of the system in the infinite cylinder geometry, which uses translational invariance to reach system sizes of $[L_y, \infty]$. Our conclusion and the following discussion are based on simulations with cylinder circumferences $L_y = 6, 12$ and $\chi \in [50, 1200]$ which we find sufficient to reach convergence.

Finite bond dimension effects and order of the phase transition

For the interacting Haldane hamiltonian given in the main text, we provide representative results in Fig. 10. They are obtain for a cut in the phase diagram for $L_y = 6$ lattice sites and $t_2/t_1 = 0.1$ as a function of V/t_1 . We show the CDW order parameter, the Hall conductivity σ_{xy} , the entanglement entropy S , and correlation length ξ/a in units of the lattice constant a of the ground-state wave-function with different $\chi \in [50, 1200]$. We compute the CDW order parameter through the ground-state expectation values of the difference of the two sub-lattice densities $\langle n_A - n_B \rangle$. The entanglement entropy S is computed by cutting the system in real space and computing the Schmidt decomposition of the groundstate, and relating the corresponding Schmidt eigenvalues to the entanglement entropy [36]. The correlation length ξ is defined as the largest decay of correlation functions, which is set by the second largest eigenvalue of the transfer matrix [36]. Finally, to obtain the Hall conductivity σ_{xy} we use the method of adiabatic flux insertion implemented numerically as detailed in Refs. [37, 49]. It consists of threading a magnetic flux through the axis of the

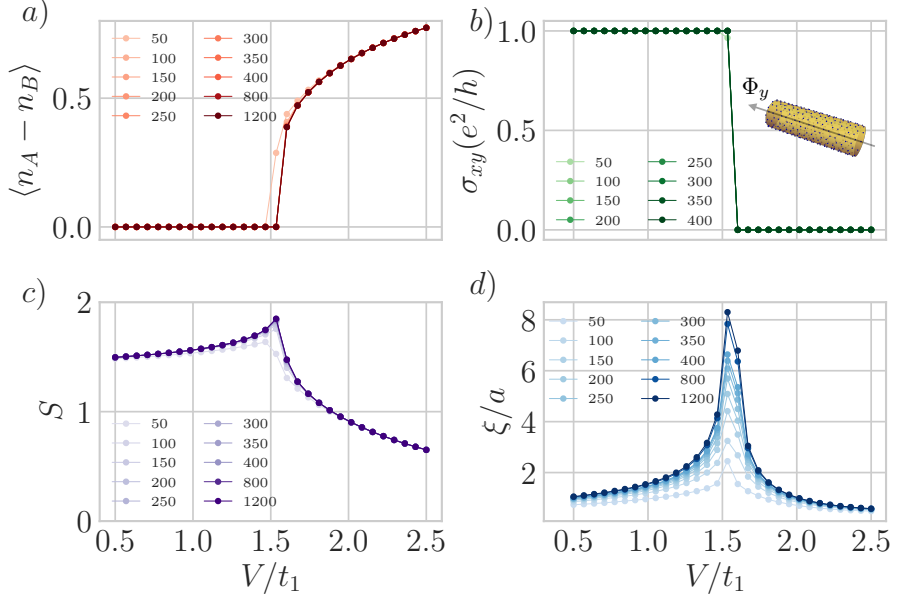


FIG. 10. iDMRG convergence. In a) the figure shows the charge density-wave order parameter. b) shows the Hall conductivity calculated by adiabatically threading a flux $\Phi_y/\Phi_0 \in [0, 2\pi]$ in units of the flux quantum Φ_0 through the cylinder geometry (inset). Within the Chern insulator or CDW phase one or zero charges are pumped leading to $\sigma_{xy} = e^2/h$ or $\sigma_{xy} = 0$ respectively. c) shows the entanglement entropy S and the figure d) shows the correlation length ξ/a in units of the lattice constant a . d) the charge density wave order parameter. Except for σ_{xy} which converges at $\chi = 100$, these quantities are calculated for bond dimensions $\chi \in [50, 1200]$ and convergence is achieved for $\chi \sim 200$.

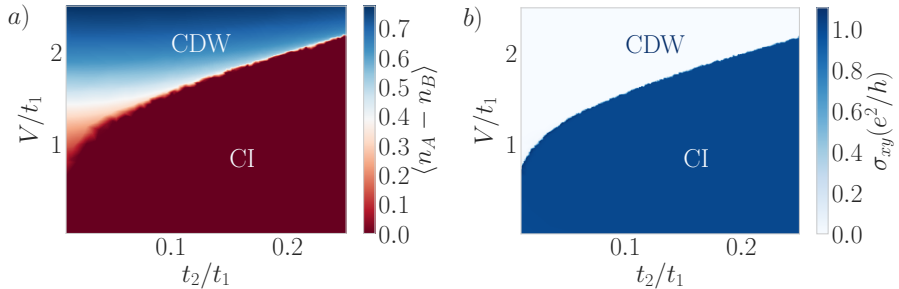


FIG. 11. Phase diagrams. a) CDW order parameter and b) σ_{xy} calculated in iDMRG for $L_y = 6$, $\chi = 200$. The phase boundary for both order parameters fall on top of each other indicating that there is no coexistence of a finite CDW order with a non-zero Hall conductivity.

cylinder by twisting the boundary conditions by a phase Φ_y (see inset in Fig. 10b)). As the flux is threaded from 0 to 2π in units of the flux quantum Φ_0 , we monitor the pumped charged through a given real-space cut of the cylinder. One charge pumped in such a cycle is equivalent to $\sigma_{xy} = e^2/h$ while no charge pumped amounts to $\sigma_{xy} = 0$ [37].

In Fig. 10 we observe that all quantities within the CI and CDW phases do not change significantly above $\chi \sim 200$, a size for the bond dimension that is consistent with previous work [37]. The topological origin of the Hall conductivity allows it to converge faster even close to the phase transition, and we find it fully converged at $\chi \sim 100$. The inverse gap in the CDW and Chern insulator phases determines the largest length scale up to which correlations spread. Thus the convergence is better as the parameters are chosen deeper in these phases, where the gap is expected to be larger, and the correlation length shorter, consistent with Fig. 10a).

In Fig. 11 we show the CDW and σ_{xy} phase diagrams for $\chi = 200$. The two phase boundaries coincide for this range of parameters; we find no intermediate phase. Although extracting the nature of the phase transition is a subtle issue in iDMRG data there are hints that this transition is first order. First, both the CDW order parameter

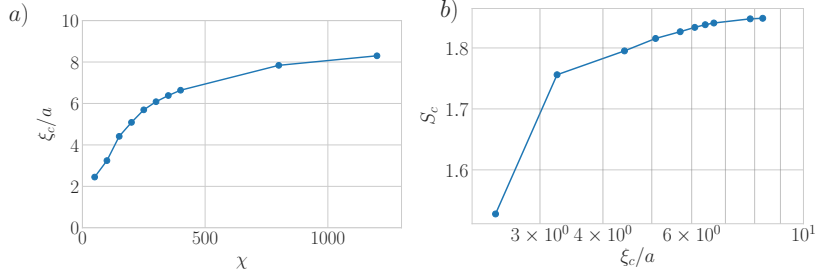


FIG. 12. Order of the phase transition in iDMRG. a) shows the correlation length at the transition ξ_c in units of the lattice constant a . A second order phase transition would show a divergent correlation length at the transition. Instead the correlation length seems to saturate with increasing χ . b) Entanglement entropy at the transition S_c plotted as a function of the correlation length at the transition ξ_c in units of the lattice constant a . The entanglement saturates as a function of correlation length, deviating from the critical scaling law $S_c = c/6 \ln(\xi_c/a) + s_0$.

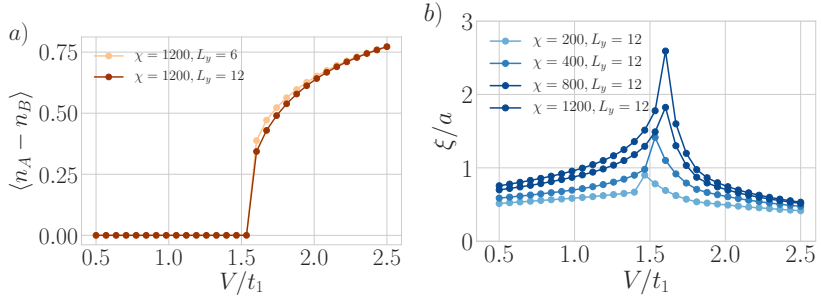


FIG. 13. Fine size effects. We show the CDW order parameter (left) and correlation length in units of the lattice constant (ξ/a , right) calculated in iDMRG for $L_y = 6$ and $L_y = 12$, and $\chi = 1200$. The phase boundary for the CDW order parameter does not change, and the correlation length drops when increasing the system size. These indicate that large system sizes lead to qualitatively the same results.

and σ_{xy} show a clear discontinuity, which can be interpreted as a first order phase transition, consistent with mean field theory. Interestingly, the correlation length ξ does not show such an evident discontinuity. We remind the reader that a second order phase transition presents a divergent correlation length ξ at the transition as a function of increasing bond dimension χ [50]. Moreover, the entanglement entropy of a critical system is expected to scale as $S = c/6 \ln(\xi/a) + s_0$ where c is the central charge and s_0 is a constant [50]. A first order phase transition on the other hand presents either a discontinuity in χ [37, 51], or a saturating behaviour of the maximal or critical correlation length, ξ_c , as a function of χ at the phase transition [52]. Our iDMRG results shown in Fig. 10 point to the latter scenario since the correlation length at the critical point seems to saturate as a function of bond dimension. This is supported by a more careful analysis, shown in Fig. 12, where we plot the maximum correlation length ξ_c as a function of χ (a), and the maximum entanglement entropy S_c as a function of ξ_c in semi-logarithmic scale (b). Both ξ_c and S_c show an increasing yet saturating behaviour, supporting the absence of a critical state with divergent correlation length. Such an increasing but non-divergent correlation length at the transition is sometimes referred to as a weak first order transition.

Finite size effects

To address the robustness of our results we have performed the calculations for $L_y = 12$ with χ up to $\chi = 1200$ (see Fig. 13) for $t_2/t_1 = 0.1$. The results are shown in Fig. 13. Fig. 13a) shows that the CDW transition is still abrupt and occurs at the same value of V/t_1 for larger system sizes. For $L_y = 12$ the correlation length ξ close to the transition presents the same peaked structure but is smaller in magnitude than that of $L_y = 6$ (see Fig. 10d)). The decrease in magnitude of ξ can be interpreted as a sign of an increase in the gap size of both the CDW and Chern insulator phases.